E9303
1/11/95

NASA
Contractor Report 195414

Army Research Laboratory
Contractor Report ARL–CR–220

Study of the Kinematic and Load Sharing Properties of Wormgearing With Non-Symmetric Tooth Profiles

D. C. Sun and Qin Yuan
State University of New York at Binghamton
Department of Mechanical and Industrial Engineering
Binghamton, New York

January 1995

Prepared for
Lewis Research Center
Under Contract NAG3–1316

National Aeronautics and
Space Administration

TABLE OF CONTENTS

Abstract ii

Nomenclature iii

1 Background and Objectives of the Study 1

2 Geometrical Features 2

2.1 Pressure Angles and Base Circles 2

2.2 Face Width of the Worm 3

2.3 Equations of Worm and Gear Surfaces on the Reverse Side 3

2.4 Tooth Depth and Tooth Top Thickness 6

3 Selection of a Feasible Non-Symmetric Tooth Profile 8

3.1 Consideration of the Distribution of Contact Lines . 8

3.2 Consideration of the Face Width of the Worm 10

3.3 A Feasible Non-Symmetric Tooth Profile 12

4 Comparison with the Symmetric Tooth Profile 12

4.1 Tooth Depth 13

4.2 Clearance between Meshing Surfaces 13

4.3 Normal Force on Gear Tooth and Worm Torque 14

4.4 Wormgear Efficiency 14

4.5 Self-Locking 15

5 Conclusion 16

References 17

Table 1 18

Figures 20

Abstract

The geometry of non-symmetric tooth profiles, i.e. tooth profiles with different pressure angles on the two sides of the tooth, is studied. A feasible non-symmetric tooth profile for application in helicopter transmissions is laid out as the best compromise among several conflicting factors. The non-symmetric tooth profile is then compared with the symmetric tooth profile studied previously. Based on the detailed comparisons it is concluded that the use of the non-symmetric tooth profile would severely limit the face width of the worm, consequently reduce the number of meshing teeth and cause much higher normal load on the individual gear teeth.

Nomenclature

(Additional wormgear nomenclature can be found in Table 1)

a	center distance of the wormgear
a_0	center distance of the first enveloping process
b_1	face width of worm
b_{1L}	face width segment defined in Fig. 2
b_{1R}	face width segment defined in Fig. 2
d	pitch diameter
d_b	diameter of base circle
i	speed ratio of the wormgear
i_0	speed ratio of the first enveloping process
N	number of teeth
N_p	number of meshing teeth
r_b	radius of base circle
T	torque
α_n	normal pressure angle
α_x	axial pressure angle
β	apex angle of the generating plane
γ	worm lead angle
η	wormgear efficiency
θ	rotation angle in the second enveloping process
μ	Coulomb friction coefficient
ψ	rotation angle in the first enveloping process
ω	rotation speed

Subscripts

$( )_1$	worm
$( )_2$	gear
$( )_W$	worm
$( )_G$	gear

Superscript

$(\dot{})$	time derivative
$( )'$	on the reverse side

1 Background and Objectives of the Study

A double-enveloping wormgear was studied in detail for possible use as an advanced helicopter transmission (Sun and Yuan, 1994, hereafter to be referred to as Report 1). The wormgear was formed by two enveloping processes: the worm surface by enveloping a family of planes created by the original generating plane that turns around the base circle (first enveloping); then the gear surface by enveloping a family of surfaces generated by the rotating worm (second enveloping). The wormgear was in the conventional form, i.e. the center distance and speed ratio were respectively the same in both the first and second enveloping processes. The dimensions and geometrical parameters of the wormgear were laid out based on the power output and speed reduction requirements of the intended application (Chaiko, 1990) and by following as closely as possible the gear standards (AGMA, 1965). These dimensions and parameters were summarized in Table 1 of Report 1 (reproduced with a few modifications in the present report also as Table 1[1]). In particular, the normal pressure angle was the conventional 20 deg as recommended by the AGMA, and the tooth profile was symmetric, i.e. the pressure angle was the same on both sides of the tooth.

Later, through discussions with the ARMY VPD personnel, it was envisaged that a smaller pressure angle on the loaded side of the tooth would be more effective in producing the needed torque; in addition, a larger tooth depth would result in a larger load bearing area hence a smaller unit load. To explore the feasibility of implementing these ideas, which represented major modifications of the conventional gear practice, we embarked on a detailed study of the non-symmetric tooth profile. The present report describes the findings of this investigation.

In the following the geometrical features of the non-symmetric tooth

[1] Some wormgear terminologies and their definitions are given in Table 1.

profile will first be described. Then a feasible non-symmetric profile is laid out which represents the best compromise among several conflicting factors. Finally the non-symmetric tooth profile will be compared with the symmetric tooth profile studied in Report 1 regarding their kinematic and load sharing properties.

2 Geometrical Features

2.1 Pressure Angles and Base Circles

There are two pressure angles: the normal pressure angle and the axial pressure angle. The two pressure angles are related through the lead angle γ (measured at the center of the worm) as follows:

$$\tan\alpha_n=(\cos\gamma)\tan\alpha_x \tag{1}$$

The base circle is defined by the axial pressure angle. Figure 1 shows their relation in the case of the symmetric profile. From the figure it is readily seen that:

$$d_b=d_2\sin(\alpha_x+\Delta\alpha)$$
$$\text{where}\quad \Delta\alpha=\frac{p_x}{2d_2} \tag{2}$$

For a non-symmetric profile the pressure angles are different on the two sides of the tooth, hence there are two base circles associated with them, Fig. 2. Here we designate the side of the tooth with a smaller axial pressure angle (hence a smaller base circle) as **the loaded side**; and the side with a larger axial pressure angle **the reverse side**. To be specific, we shall distinguish the axial pressure angles of the two sides by means of a center line (od) which runs through the center of the gear and the midpoint of the tooth space on the gear pitch circle, as depicted in Fig. 2. The properties associated with the reverse side will be denoted by ( )'.

2.2 Face Width of the Worm

The face width of the worm is the active part of the pinion face; it should be long enough to contain the needed number of meshing teeth for sharing the load. However, the face width must not be greater than the diameter of the base circle, otherwise tooth interference would occur on that part of the worm extending beyond the diameter of the base circle. For symmetric tooth profiles with standard normal pressure angles, formulas such as $b_1 \leq d_b - 0.1a$ (AGMA, 1965) and $b_1 \leq d_b - 0.03a$ (Dudley, 1984) are recommended for the face width. In the case of the non-symmetric profile there are two base circles. It is convenient to consider the face width as containing two segments, $b_1 = b_{1L} + b_{1R}$, where b_{1L} is the segment corresponding to the smaller base circle and b_{1R} the segment corresponding to the larger base circle, as shown in Fig. 2. Clearly then b_{1L} should be smaller than r_b and b_{1R} should be smaller than r_b'. As a result the face width is shortened and, in the case of very small α_n, may not contain enough meshing teeth. It should also be cautioned that though b_{1R} can be nearly as large as the radius of the larger base circle, the teeth toward the end of the meshing zone may not be effective in sharing the load. This is because the second enveloping contact lines on these teeth may not exist, as was explained in Report 1 and shown by Figs. 3.7(e)-(f) therein.

2.3 Equations of Worm and Gear Surfaces on the Reverse Side

Report 1 contains the equations of the worm and gear surfaces only for the loaded side. This is because in the symmetric tooth profile the reverse side is just the mirror image of the loaded side. Since we now deal with the non-symmetric tooth profile, the mathematical expressions for the surfaces on the reverse side need be derived anew. In the following derivations the methodology, coordinate systems and nomenclature are the same as those employed in Report 1.

2.3.1 The Original Generating Plane

Suppose the original generating plane for the loaded side tangents the base circle at point a, say, $\psi_2 = \psi_s$, as shown in Fig. 2. Then the original generating plane for the reverse side tangents its base circle at point a', where $\psi_2 = \psi_s + \pi - \varepsilon$, and

$$\varepsilon = \pi - \sin^{-1}\frac{d_b}{d_2} - \sin^{-1}\frac{d_b'}{d_2} + \frac{2S_1}{d_2} \tag{3}$$

and the equation of the plane is given in S_2 as:

$$f'=x_2'\sin\varepsilon+y_2'\cos\varepsilon-z_2'\tan\beta-r_b'=0 \tag{4}$$

2.3.2 The Worm Surface

After coordinate transformation of Eq. 4 into S_1, a family of planes is obtained:

$$\begin{aligned} F'=A_\psi^{(12)}f'=&x_1'(\cos\psi_1\sin(\psi_2-\varepsilon)+\tan\beta\sin\psi_1)\\ &+y_1'(-\sin\psi_1\sin(\psi_2-\varepsilon)+\tan\beta\cos\psi_1)\\ &-z_1'\cos(\psi_2-\varepsilon)-(a_0\sin(\psi_2-\varepsilon)+r_b') = 0 \end{aligned} \tag{5}$$

The envelope of this family of planes, which is the worm surface, is given jointly by Eq. 5 and the following equation:

$$\begin{aligned} D_\psi F'=&x_1'(\cos\psi_1\cos(\psi_2-\varepsilon)+i_0\tan\beta\cos\psi_1-i_0\sin\psi_1\sin(\psi_2-\varepsilon))\\ &+y_1'(-\sin\psi_1\cos(\psi_2-\varepsilon)-i_0\tan\beta\sin\psi_1-i_0\cos\psi_1\sin(\psi_2-\varepsilon))\\ &+z_1'\sin(\psi_2-\varepsilon)-a_0\cos(\psi_2-\varepsilon) = 0 \end{aligned} \tag{6}$$

2.3.3 The Gear Surface

By comparing Eqs. 5 and 6 in the above with Eqs. 18 in Report 1, it is

seen that the expression for the worm surface on the reverse side is the same as that on the loaded side provided the quantities ψ_2 and r_b in the latter are replaced by $(\psi_2 - \varepsilon)$ and $(-r_b')$ respectively. Hence the expression for the gear surface on the reverse side can be obtained directly from that on the loaded side, Eqs. 27-31 in Report 1, with such substitutions. Thus, the gear surface is given by:

$$\begin{aligned} A_\theta^{(21)} F' &= 0 \\ A_\theta^{(21)} D_\psi F' &= 0 \\ A_\theta^{(21)} D_\theta^{(1)} F' &= 0 \end{aligned} \tag{7}$$

or

$$\begin{bmatrix} a_{11} & a_{12} & a_{13} & a_{14} \\ a_{21} & a_{22} & a_{23} & a_{24} \\ a_{31} & a_{32} & a_{33} & a_{34} \\ 0 & 0 & 0 & 1 \end{bmatrix} \begin{bmatrix} x_2' \\ y_2' \\ z_2' \\ 1 \end{bmatrix} = \begin{bmatrix} 0 \\ 0 \\ 0 \\ 1 \end{bmatrix} \tag{8}$$

where

$$\begin{aligned} a_{11} &= -\sin(\psi_2-\varepsilon)\cos\theta_2\cos(\psi_1-\theta_1) - \tan\beta\cos\theta_2\sin(\psi_1-\theta_1) + \cos(\psi_2-\varepsilon)\sin\theta_2 \\ a_{12} &= \sin(\psi_2-\varepsilon)\sin\theta_2\cos(\psi_1-\theta_2) + \tan\beta\sin\theta_2\sin(\psi_1-\theta_1) + \cos(\psi_2-\varepsilon)\cos\theta_2 \\ a_{13} &= \sin(\psi_2-\varepsilon)\sin(\psi_1-\theta_1) - \tan\beta\cos(\psi_1-\theta_1) \\ a_{14} &= a\,[\sin(\psi_2-\varepsilon)\cos(\psi_1-\theta_1) + \tan\beta\sin(\psi_1-\theta_1)] - a_0\sin(\psi_2-\varepsilon) - r_b' \end{aligned} \tag{9}$$

$$\begin{aligned} a_{21} &= \sin(\psi_2-\varepsilon)\cos\theta_2\sin(\psi_1-\theta_1) - \tan\beta\cos\theta_2\cos(\psi_1-\theta_1) \\ &\quad -[\sin(\psi_2-\varepsilon)\sin\theta_2 + \cos(\psi_2-\varepsilon)\cos\theta_2\cos(\psi_1-\theta_1)]/i_0 \\ a_{22} &= -\sin(\psi_2-\varepsilon)\sin\theta_2\sin(\psi_1-\theta_1) + \tan\beta\sin\theta_2\cos(\psi_1-\theta_1) \\ &\quad -[\sin(\psi_2-\varepsilon)\cos\theta_2 - \cos(\psi_2-\varepsilon)\sin\theta_2\cos(\psi_1-\theta_1)]/i_0 \\ a_{23} &= \sin(\psi_2-\varepsilon)\cos(\psi_1-\theta_1) + \tan\beta\sin(\psi_1-\theta_1) \\ &\quad +[\cos(\psi_2-\varepsilon)\sin(\psi_1-\theta_1)]/i_0 \\ a_{24} &= -a\,[\sin(\psi_2-\varepsilon)\sin(\psi_1-\theta_1) - \tan\beta\cos(\psi_1-\theta_1) \\ &\quad -\cos(\psi_2-\varepsilon)\cos(\psi_1-\theta_1)/i_0] - a_0\cos(\psi_2-\varepsilon)/i_0 \end{aligned} \tag{10}$$

$$
\begin{aligned}
a_{31} &= a_{12} - i[\sin(\psi_2-\varepsilon)\cos\theta_2\sin(\psi_1-\theta_1) - \tan\beta\cos\theta_2\cos(\psi_1-\theta_1)] \\
a_{32} &= -a_{11} + i[\sin(\psi_2-\varepsilon)\sin\theta_2\sin(\psi_1-\theta_1) - \tan\beta\sin\theta_2\cos(\psi_1-\theta_1)] \\
a_{33} &= -i[\sin(\psi_2-\varepsilon)\cos(\psi_1-\theta_1) + \tan\beta\sin(\psi_1-\theta_1)] \\
a_{34} &= ai[\sin(\psi_2-\varepsilon)\sin(\psi_1-\theta_1) - \tan\beta\cos(\psi_1-\theta_1)]
\end{aligned}
\qquad (11)
$$

2.4 Tooth Depth and Tooth Top Thickness

Tooth depth is a basic parameter that affects many other gear dimensions. The standard tooth depth and clearance are given in Table 1 in terms of coefficients k_e and k_c, where $k_e = 0.225$ and $k_c = 0.05$. Tooth depth can be increased by making these coefficients greater than their standard values. However, the increase of tooth depth is restricted by at least two factors. One is that tooth undercut should be avoided. The other is that a minimum tooth top thickness should be maintained, a recommended formula being $S_a \geq 0.15x_m$ (Shen, et al., 1983).

A difference between the non-symmetric and symmetric tooth profiles regarding the tooth thickness should be noted. Since the axial pitch is the same, the tooth thickness at the pitch circle is the same in both profiles. However, since the axial pressure angle on the loaded side is smaller in the non-symmetric profile, the tooth top thickness is greater, and the tooth root thickness is less, than the corresponding thicknesses in the symmetric profile. Hence, if the top thickness were the only concern, then tooth depth could be made greater in the case of the non-symmetric profile.

The (axial) top thickness of the worm thread, S_{a1}, can be obtained analytically. The top of the thread on the loaded side can be found by solving the following set of equations:

$$F=0,\quad DF=0,\quad y_1=0$$
$$(a-x_1)^2+z_1^2=(0.5d_{f2}+c)^2 \tag{12}$$

Likewise the top of the thread on the reverse side can be found by solving:

$$F'=0,\quad DF'=0,\quad y_1'=0$$
$$(a-x_1')^2+z_1'^2=(0.5d_{f2}+c)^2 \tag{13}$$

The distance between the two points is S_{a1}. Note that the top thickness of the thread becomes progressively small toward the ends of the worm. Besides, the top thickness in the normal direction is smaller than S_{a1} by a factor of $(\cos\gamma)$.

The tooth thickness of the gear is the smallest at the mid-plane ($z_2 = 0$), as can be readily seen from Fig. 3.4 in Report 1. To check the (axial) tooth top thickness of the gear analytically, one can similarly solve the following sets of equations:

$$A_\theta^{(21)}F=0,\quad A_\theta^{(21)}D_\psi F=0,\quad A_\theta^{(21)}D_\theta^{(1)}F=0,$$
$$z_2=0,\quad x_2^2+y_2^2=(0.5d_{a2})^2 \tag{14}$$

$$A_\theta^{(21)}F'=0,\quad A_\theta^{(21)}D_\psi F'=0\quad A_\theta^{(21)}D_\theta^{(1)}F'=0,$$
$$z_2'=0,\quad x_2'^2+y_2'^2=(0.5d_{a2})^2 \tag{15}$$

for the top points on the two sides of the gear tooth and then find the distance between them. The top thickness in the normal direction is then given by $S_{a2}(\cos\gamma)$.

The above sets of equations are solved to obtain the worm and gear tooth profiles in the mid-plane. Once the tooth profiles are plotted, by visual observation one can determine whether there is undercut and whether there is room to extend the tooth depth. Our later discussion of the tooth depth issue will be based on visual observation of the worm tooth profiles so obtained.

3 Selection of a Feasible Non-Symmetric Tooth Profile

In this section we search for an acceptable set of geometrical parameters for the loaded side, that include the normal pressure angle (α_n), the apex angle (β), and the face width of the worm (b_1). For the reverse side the normal pressure angle (α_n') remains to be 20 deg as adopted in Report 1.

3.1 Consideration of the Distribution of Contact Lines

Contact lines form the worm and gear surfaces, from which most contact properties can be determined. Hence, the distribution of contact lines should first be investigated when one searches for a new geometry. From the point of view of maximizing the contact area and to even out tooth wear, a desirable distribution of contact lines would be one where the contact lines are spread evenly on the tooth flank. To approach such a contact situation one needs to adjust several geometrical parameters, among which the most influential ones are α_n and β.

Consider the case of α_n = 20 deg. Figures 3-5 show the distributions of contact lines on a gear tooth, as viewed in the (x_2, z_2) plane, for three β values, viz. 1.5 deg, 3.75 deg, and 7.5 deg. The other dimensions and parameters are the same as in Report 1. Each of the figures amounts to the superposition of a series of snap shots of the contact lines as the gear tooth runs through the meshing zone. In Fig. 3 β is less than γ (2.533 deg), the region occupied by the first enveloping contact lines lies above the one

occupied by the second enveloping contact lines. In Figs. 4 and 5 β is greater than γ and the reverse is true. These regions, occupied respectively by the first and second enveloping contact lines, represent the areas on the gear tooth that experience contact with the worm. In Fig. 3 the contact regions crowd around the mid-plane but leave a gap between them without contact lines. As β increases (Figs. 4 and 5), the contact regions grow and cover more of the tooth flank.

For the sake of comparison the distribution of contact lines, as viewed in the (x_2, z_2) plane, in the case studied in Report 1 (β = 5 deg) is shown in Fig. 6. Figure 7 is the view in the (y_2, z_2) plane of these contact lines. Since the first enveloping contact lines form the planar part of the gear surface which runs parallel to the x_2 axis, this part of the tooth flank appears as a straight line in the (y_2, z_2) plane. The second enveloping contact lines form the curved part of the gear surface which does not run parallel to the x_2 axis, hence these contact lines still appear as curves in the (y_2, z_2) plane.

Figures 8-10 show the distributions of contact lines for the same set of β values (1.5 deg, 3.75 deg, and 7.5 deg) as in Figs. 3-5, but for α_n = 8.5 deg. The other dimensions and parameters are the same as in Report 1, except that N_p = 6. It can be seen that the effect of decreasing α_n is to move the (first and second) contact regions apart and away from the mid-plane. The case of α_n = 8.5 deg and β = 5 deg is shown in Figs. 11-12. A comparison of Figs. 11-12 with Figs. 6-7 further demonstrates this effect. It is seen that for different pressure angles one can select different apex angles to obtain the desired distribution of contact lines. Thus, β = 5 deg is better for α_n = 20 deg; whereas β= 3.75 deg appears better for α_n = 8.5 deg.

The distribution of contact lines is also affected by the pitch diameter of the worm, because the latter locates the tooth domains on the worm and gear

surfaces. Figure 13 shows a case of α_n = 8.5 deg, β= 7.5 deg and d_1 = 200 mm. By comparing with Fig. 10, one can see that β = 7.5 deg is a good choice for this case.

3.2 Consideration of the Face Width of the Worm

As mentioned earlier the face width of the worm should be less than the base circle diameter to avoid tooth interference and in the meanwhile should be long enough to contain the needed number of meshing teeth for load sharing. The relation between the face width and the number of meshing teeth is given by Shen, et al. (1983) as:

$$b_1 = d_2 \sin\psi_a$$
$$\text{where} \quad \psi_a = \pi (N_p - 0.45)/N_2 \tag{16}$$

The AGMA recommended values of N_p = 5 and α_n = 20 deg are usually compatible with the above requirements. For a highly loaded wormgear N_p need be increased so as to reduce the load level on the individual teeth. This demand conflicts with the one of decreasing the normal pressure angle which would result in a shorter face width. Another factor that restricts the face width is the top thickness of the worm thread, which becomes progressively small toward the ends of the worm.

To see that tooth interference occurs when the face width is longer than the base circle diameter, let us consider the hypothetical case of α_n=0 deg and all the other dimensions being the same as in Report 1. The base circle radius on the loaded side, r_b, in this case is less than 30 mm. The contact lines on a gear tooth are shown in Figs. 14-15. As viewed in the (x_2, z_2) plane, Fig. 14, two sets of contact lines overlap each other. If viewed in the (y_2, z_2) plane, Fig. 15, the two sets are located respectively on the two sides of a dashed line (which is drawn for the convenience of discussion). The set on the left of the dashed line are generated by the enveloping

processes between the gear and the b_{1R} segment of the worm (Fig. 2) and are exterior (so termed because the interior of the gear body is on the right of the contact lines) to the other set, which are generated by the enveloping processes between the gear and the b_{1L} segment of the worm. Recall that the enveloping processes are also the machining processes during manufacturing. Thus, with the presence of the b_{1L} segment of the worm, the exterior contact lines can not exist because this part of the gear body is actually machined off. Besides, the gear surface formed by the contact lines on the right of the dashed line is convex (Fig. 15) and does not wrap around the worm surface. Hence, the exterior contact lines are the desired ones, which would be destroyed by the presence of the b_{1L} segment of the worm.

Of course, tooth interference can be avoided if one removes the b_{1L} segment of the worm and extends the b_{1R} segment up to r_b'. However, as explained in Section 2.2, the teeth toward the end of the meshing zone may not be effective in sharing the load. Hence, one is in fact left with half of a worm. Figures 16-17 show such a case, where N_p is reduced to half of its original value. Therefore, the idea of a truncated worm can not maintain the required N_p value and is not acceptable. We shall henceforth consider only the situation that the worm is symmetric with respect to its center.

Figures 18-19 show the case of α_n = 8.5 deg, β = 3.5 deg and N_p = 6; other dimensions being the same as in Report 1. In this case the face width of the worm is 230.0 mm, which is very close to the base circle diameter (236.6 mm). From the distribution of contact lines it can be seen that tooth interference still occurs, but only when the gear and worm begin to mesh, i.e. when the left end of the worm encounters the two ends of the gear tooth away from the mid-plane. This minor interference can be removed by slightly reducing the face width of the worm. An alternative is to slightly increase the apex angle. For instance, no interference is present in Figs. 11-12, where β = 5 deg. This is because, with a larger β, the top thickness of the

worm thread is reduced, then the part of the worm thread that interferes with the gear tooth is eliminated.

The requirement of maintaining a minimum tooth top thickness also places a restriction on the face width, because the top thickness of the worm thread becomes progressively small toward the ends of the worm. This is clearly shown in Figs. 20-21 for the case of α_n = 20 deg, N_p = 10; and in Figs. 22-23 for the case of α_n = 8.5 deg, N_p = 6. These figures also demonstrate vividly the effect of increasing β in making the tooth top thickness small.

3.3 A Feasible Non-Symmetric Tooth Profile

From the above analysis one may draw the following conclusions: (1) A small normal pressure angle limits the face width of the worm, which in turn limits the number of meshing teeth. For a highly loaded wormgear it is desirable to have a large number of meshing teeth. Hence, the normal pressure angle may not be chosen arbitrarily small. (2) At any given normal pressure angle, it appears always possible to find an apex angle that produces an evenly distributed contact lines. (3) Increasing the apex angle is helpful in removing tooth interference, but it also has the undesirable effect of causing the tooth top thickness small.

The above considerations have led to a compromised choice of the non-symmetric tooth profile, in which α_n = 8.5 deg, β = 3.75 deg, N_p = 6; and all the other dimensions and parameters are as adopted in Report 1.

4 Comparison with the Symmetric Tooth Profile

In this section the non-symmetric tooth profile chosen in Section 3.3 is compared with the symmetric tooth profile studied in Report 1 regarding their kinematic and load sharing properties.

4.1 Tooth Depth

Figures 20 and 22 show that, at a small β value (1.5 deg), there is some room (though very limited) for extending the tooth depth, but the relative merit between the two profiles in this regard is not obvious. At a large β value (7.5 deg), Figs. 21 and 23 show that the tooth top is already quite sharp in both profiles, and there is no possibility to extend the tooth depth.

4.2 Clearance between Meshing Surfaces

The shape of the clearance is crucial to the implementation of fluid film lubrication. Since the worm and gear teeth are in line contact instead of area contact, the best one can hope for is that the relative curvatures transverse to the contact lines be small, so that large, relatively flat regions exist around the contact lines to serve as the load bearing areas of the oil films. The clearance is a complicated function not only of the position on a tooth flank but also of time. It is only possible to show some representative results as an illustration of the clearance shape in the two tooth profiles. In the following the situation on the second contact tooth in the non-symmetric profile and that on the fourth contact tooth in the symmetric profile will be shown. The two situations are equivalent because in the former case there are six pairs of contact teeth in the meshing zone whereas in the latter case there are ten pairs. Figure 24 depicts six arbitrarily chosen sections on the tooth flank where the clearance function will be shown. Figures 25-27 show, in the case of the symmetric tooth profile, the clearance function at sections x_I, x_{II} and x_{III} as viewed in the (y_2, z_2) plane; and Fig. 28 the clearance function at sections z_I, z_{II} and z_{III} as viewed in the (x_2, y_2) plane. The analogous situations in the case of the non-symmetric tooth profile are shown in Figs. 29-32.

From these figures it is seen that two regions, one on each side of the

mid-plane, can be identified as the areas for implementing fluid film lubrication. The results also show a feature, which is unfavorable to fluid film lubrication, that the clearance grows quickly as the distance from a contact line increases. However, both these features are present in the two tooth profiles, and the relative merit between them is not obvious.

4.3 Normal Force on Gear Tooth and Worm Torque

According to the hypothesis of load sharing (described in Report 1), the load acting on a gear tooth is proportional to the length of contact lines on the tooth. Once the total load is prescribed, it is shared by the meshing teeth according to the length of contact lines on each tooth. In the non-symmetric tooth profile there are six pairs of meshing teeth, as a result the load level on the individual teeth is much higher than that in the symmetric tooth profile, which has ten pairs of meshing teeth. This is shown in Fig. 33. Likewise the worm torque distributed along the worm tooth is compared in Fig. 34 between the two profiles. In these comparisons a Coulomb friction coefficient of 0.07 is used, which is a typical value when full film lubrication is not established at the contact. From these comparisons it is seen that the price paid for having a smaller pressure angle is considerable.

4.4 Wormgear Efficiency

The load level in the two profiles are further compared based on both having the same number of meshing teeth, viz. $N_p = 6$. Figures 35 and 36 show that the non-symmetric tooth profile generally displays a lower level of gear load and worm torque. But the difference is not pronounced, in other words, the smaller pressure angle does not appear as effective as one expects in producing the needed gear torque. To see why this is the case, let us examine the wormgear efficiency.

The wormgear efficiency may be defined as the ratio of the worm torque without friction to that with friction:

$$\eta = \frac{T_W}{T_{fW}} \tag{17}$$

The formulas for T_w and T_{fW} (along with the formulas for $F_{Gm}{}^n$ and $F_{fGm}{}^n$ needed to evaluate them) are given in Section 4.2 (and Section 4.3) of Report 1. For the purpose of illustration, let us simplify these expressions by taking only one term (the contribution from the thread at the center of the worm) in each of the summation signs. Recognizing that $x_p = d_1/2$; $z_p = 0$; $a = (d_1 + d_2)/2$; $n_W = 1$; $|n_{jy}| = (\cos \alpha_n)(\sin \gamma)$; $|n_{jz}| = (\cos \alpha_n)(\cos \gamma)$; and $\tan \gamma = d_2\omega_2/d_1\omega_1$, Eq. 17 is reduced to:

$$\eta \sim \frac{\cos\alpha_n - \mu \tan\gamma}{\cos\alpha_n + \mu \cot\gamma} \tag{18}$$

which is actually the efficiency of the cylindrical wormgear (Shigley and Mitchell, 1983, p.652). With $\gamma = 2.533$ deg and $\mu = 0.07$, the efficiency is found to be $\eta = 0.386$ ($\alpha_n = 0$ deg); $\eta = 0.383$ ($\alpha_n = 8.5$ deg); and $\eta = 0.371$ ($\alpha_n = 20$ deg). Hence, the normal pressure angle does not significantly affect the efficiency.

4.5 Self-Locking

The question of self-locking arises because during the operation of the transmission the situation of a stalled engine may be encountered. Under that circumstance the worm associated with the stalled engine would be driven by the gear, i.e. the reverse side of the worm thread would be driven by the reverse side of the gear tooth. Self-locking is analogous to the situation where a weight is prevented from sliding down an inclined plane by friction. This occurs when the friction coefficient is greater than the tangent of the angle of inclination, and the weight is said to be subjected to self-locking. The criterion for the self-locking of the wormgear can be obtained by

considering the efficiency of the weight (corresponding to the gear) in pushing away the inclined plane (corresponding to the worm):

$$\eta = \frac{\textit{weight without friction}}{\textit{weight with friction}} \tag{19}$$

with an effective friction coefficient $\mu/(\cos \alpha_n')$ (Shigley and Mitchell, 1983, p.365). The expression for this efficiency can be readily derived:

$$\eta = \frac{\cos\alpha_n' - \mu \cot\gamma}{\cos\alpha_n' + \mu \tan\gamma} \tag{20}$$

The wormgear is self-locked if this efficiency is zero or negative, i.e.

$$\mu \geq (\cos\alpha_n')(\tan\gamma) \tag{21}$$

For the studied wormgear ($\gamma = 2.533$ deg), the friction coefficient must be less than $0.0442(\cos \alpha_n')$ to avoid self-locking when it is driven in reverse. Since the friction coefficient in unlubricated contacts is most likely greater than this value, fluid film lubrication is needed for the reverse side.

There is no difference between the symmetric and non-symmetric tooth profiles regarding self-locking because on the reverse side they are the same ($\alpha_n' = 20$ deg).

5 Conclusion

Based on the above studies of the geometry of non-symmetric tooth profiles, i.e. tooth profiles with different pressure angles on the two sides of the tooth, and the detailed comparisons between a feasible non-symmetric tooth profile and the symmetric tooth profile studied previously, it is concluded that the use of the non-symmetric profile would severely limit the face width of the worm, consequently reduce the number of meshing teeth and cause much higher normal load on the individual gear teeth. While the non-symmetric profile effects a somewhat higher wormgear efficiency, this little gain cannot offset the penalty of its use. Since the success of the wormgear

transmission hinges on the establishment of fluid film lubrication at the contact, and the latter task would be made easier with a lower contact load, it is recommended that the symmetric tooth profile, with a large number of meshing teeth, be adopted for further lubrication studies.

References

American Gear Manufactures Association, 1965, "Design of General Industrial Double-Enveloping Wormgears", AGMA Standard 342.02.

Chaiko, L., 1990, "Assessment of Worm Gearing for Helicopter Transmissions", NASA Technical Memorandum 102441, AVSCOM Technical Memorandum 89-C-010.

Dudley, D. W., 1984, Handbook of Practical Gear Design, McGraw-Hill.

Shen, Y. F. et al., 1983, Meshing of Spatial Mechanisms and the SG-71 Wormgear (in Chinese), Metallurgy Industry Publication Corporation, Beijing.

Shigley, J. E. and Mitchell, L. D., 1983, Mechanical Engineering Design, 4th Ed., McGraw-Hill.

Sun, D. C. and Yuan, Q., 1994, "Study of the Kinematic and Dynamic Characteristics of a Wormgear Transmission for Helicopter Applications", NASA Contractor Report 195287, Army Research Laboratory Contractor Report-ARL-CR-78.

Table 1 Dimensions of the Wormgear Studied in Report 1

TERM	SYMBOL	VALUE	FORMULA BASED	REFERENCE
speed ratio	i	110		given
normal pressure angle (loaded side)	α_n	20 deg		Dudley, 1984 p. 3.71
normal pressure angle (reverse side)	α_n'	20 deg		Dudley, 1984 p. 3.71
center distance	a	880 mm		selected
number of worm threads	N_1	1		selected
number of gear teeth	N_2	110	$N_2 = N_1*i$	
pitch diameter of worm*	d_1	300 mm	$d_1 = a^{0.875}/k_d$ (k_d = 1.7~2.2)	Dudley, 1984 p. 3.70
pitch diameter of gear	d_2	1460 mm	$d_2 = 2*a-d_1$	
axial pitch	p_x	41.6975 mm	$p_x = \pi*d_2/N_2$	Dudley, 1984 Table 3.32
worm lead angle*	γ	2.533 deg	$\tan\gamma = p_x*N_1/\pi/d_1$	Dudley, 1984 Eq. 3.38
normal circular pitch	p_n	41.6568 mm	$p_n = p_x*\cos\gamma$	Dudley, 1984 Table 3.32
axial pressure angle*	α_x	20.018 deg	$\tan\alpha_x = \tan\alpha_n/\cos\gamma$	Dudley, 1984 Eq. 3.40
	$\Delta\alpha$	0.818 deg	$\Delta\alpha = p_x/2/d_2$	Dudley, 1984 p. 3.72
base circle diameter	d_b	519.3182 mm	$d_b = d_2*\sin(\alpha_x+\Delta\alpha)$	Dudley, 1984 Eq. 3.41
module	x_m	13.2727 mm/tooth	$x_m = p_x/\pi$	Dudley, 1984 Table 3.32
number of meshing teeth	N_p	10		selected
half angle of meshing	ψ_a	15.627 deg	$\psi_a = \pi*(N_p-0.45)/N_2$	Shen, 1983 Table 10.1
start angle of meshing	ψ_f	5.209 deg	$\psi_f = \sin^{-1}(d_b/d_2)-\psi_a$	Shen, 1983 Table 10.1
thickness of worm thread	S_1	18.7639 mm	$S_1 = 0.45*p_x$	Dudley, 1984 p. 3.73

thickness of gear tooth	S_2	22.9336 mm	$S_2 = 0.55*p_x$	Dudley, 1984 P. 3.73
whole depth	b_t	20.8284 mm	$b_t = b_k+c$	Dudley, 1984 Table 3.31
working depth	b_k	18.7455 mm	$b_k = 2*b_a$	Dudley, 1984 Table 3.31
addendum	b_a	9.3728 mm	$b_a = k_e*p_n$ ($k_e = 0.225$)	Dudley, 1984 Table 3.31
clearance	c	2.0829 mm	$c = k_c*p_n$ ($k_c = 0.05$)	
throat diameter of worm*	d_{a1}	318.7455 mm	$d_{a1} = d_1+2*b_a$	Shen, 1983 Table 10.1
root diameter of worm*	d_{f1}	277.0888 mm	$d_{f1} = d_{a1}-2*b_t$	Dudley, 1984 Eq. 3.39
throat diameter of gear	d_{a2}	1478.7455 mm	$d_{a2} = d_2+2*b_a$	Dudley, 1984 Table 3.32
root diameter of gear	d_{f2}	1437.0888 mm	$d_{f2} = d_{a2}-2*b_t$	Shen, 1983 Table 10.1
face width of worm	b_1	393 mm	$b_1 = d_2*\sin\psi_a$	Shen, 1983 Table 10.1
face width of gear	b_2	249 mm	$b_2 = (0.9\sim1.0)*d_{f1}$	Shen, 1983 Table 10.1
apex angle of generating plane	β	5 deg		selected

* At the center of worm.

Figures

Fig. 1 Symmetric tooth profile

Fig. 2 Non-symmetric tooth profile

Fig. 3 Distribution of contact lines on a gear tooth
α_n = 20 deg, β = 1.5 deg, N_p = 10, d_1 = 300 mm

Fig. 4 Distribution of contact lines on a gear tooth
α_n = 20 deg, β = 3.75 deg, N_p = 10, d_1 = 300 mm

Fig. 5 Distribution of contact lines on a gear tooth
α_n = 20 deg, β = 7.5 deg, N_p = 10, d_1 = 300 mm

Fig. 6 Distribution of contact lines on a gear tooth
α_n = 20 deg, β = 5 deg, N_p = 10, d_1 = 300 mm

Fig. 7 Distribution of contact lines on a gear tooth
α_n = 20 deg, β = 5 deg, N_p = 10, d_1 = 300 mm

Fig. 8 Distribution of contact lines on a gear tooth
α_n = 8.5 deg, β = 1.5 deg, N_p = 6, d_1 = 300 mm

Fig. 9 Distribution of contact lines on a gear tooth
α_n = 8.5 deg, β = 3.75 deg, N_p = 6, d_1 = 300 mm

Fig. 10 Distribution of contact lines on a gear tooth
α_n = 8.5 deg, β = 7.5 deg, N_p = 6, d_1 = 300 mm

Fig. 11 Distribution of contact lines on a gear tooth
α_n = 8.5 deg, β = 5 deg, N_p = 6, d_1 = 300 mm

Fig. 12 Distribution of contact lines on a gear tooth
α_n = 8.5 deg, β = 5 deg, N_p = 6, d_1 = 300 mm

Fig. 13 Distribution of contact lines on a gear tooth
α_n = 8.5 deg, β = 7.5 deg, N_p = 6, d_1 = 200 mm

Fig. 14 Distribution of contact lines on a gear tooth
α_n = 0 deg, β = 5 deg, N_p = 10, d_1 = 300 mm

Fig. 15 Distribution of contact lines on a gear tooth
α_n = 0 deg, β = 5 deg, N_p = 10, d_1 = 300 mm

Fig. 16 Distribution of contact lines on a gear tooth
(same parameters as in Fig. 14 except b_{1L} = 0)

Fig. 17 Distribution of contact lines on a gear tooth
(same parameters as in Fig. 15 except b_{1L} = 0)

Fig. 18 Distribution of contact lines on a gear tooth
α_n = 8.5 deg, β = 3.5 deg, N_p = 6, d_1 = 300 mm

Fig. 19 Distribution of contact lines on a gear tooth
α_n = 8.5 deg, β = 3.5 deg, N_p = 6, d_1 = 300 mm

Fig. 20 Worm tooth profile in the mid-plane
α_n = 20 deg, β = 1.5 deg, N_p = 10, d_1 = 300 mm

Fig. 21 Worm tooth profile in the mid-plane
α_n = 20 deg, β = 7.5 deg, N_p = 10, d_1 = 300 mm

Fig. 22 Worm tooth profile in the mid-plane
α_n = 8.5 deg, β = 1.5 deg, N_p = 6, d_1 = 300 mm

Fig. 23 Worm tooth profile in the mid-plane
α_n = 8.5 deg, β = 7.5 deg, N_p = 6, d_1 = 300 mm

Fig. 24 Sections where the clearance function is shown

Fig. 25 Clearance function at x_I (α_n = 20 deg)

Fig. 26 Clearance function at x_{II} (α_n = 20 deg)

Fig. 27 Clearance function at x_{III} (α_n = 20 deg)

Fig. 28 Clearance function at z_I, z_{II} and z_{III} (α_n = 20 deg)

Fig. 29 Clearance function at x_I (α_n = 8.5 deg)

Fig. 30 Clearance function at x_{II} (α_n = 8.5 deg)

Fig. 31 Clearance function at x_{III} (α_n = 8.5 deg)

Fig. 32 Clearance function at z_I, z_{II} and z_{III} (α_n = 8.5 deg)

Fig. 33 Comparison of normal force acting on a gear tooth

Fig. 34 Comparison of worm torque distribution along the worm tooth

Fig. 35 Comparison of normal force acting on a gear tooth

Fig. 36 Comparison of worm torque distribution along the worm tooth

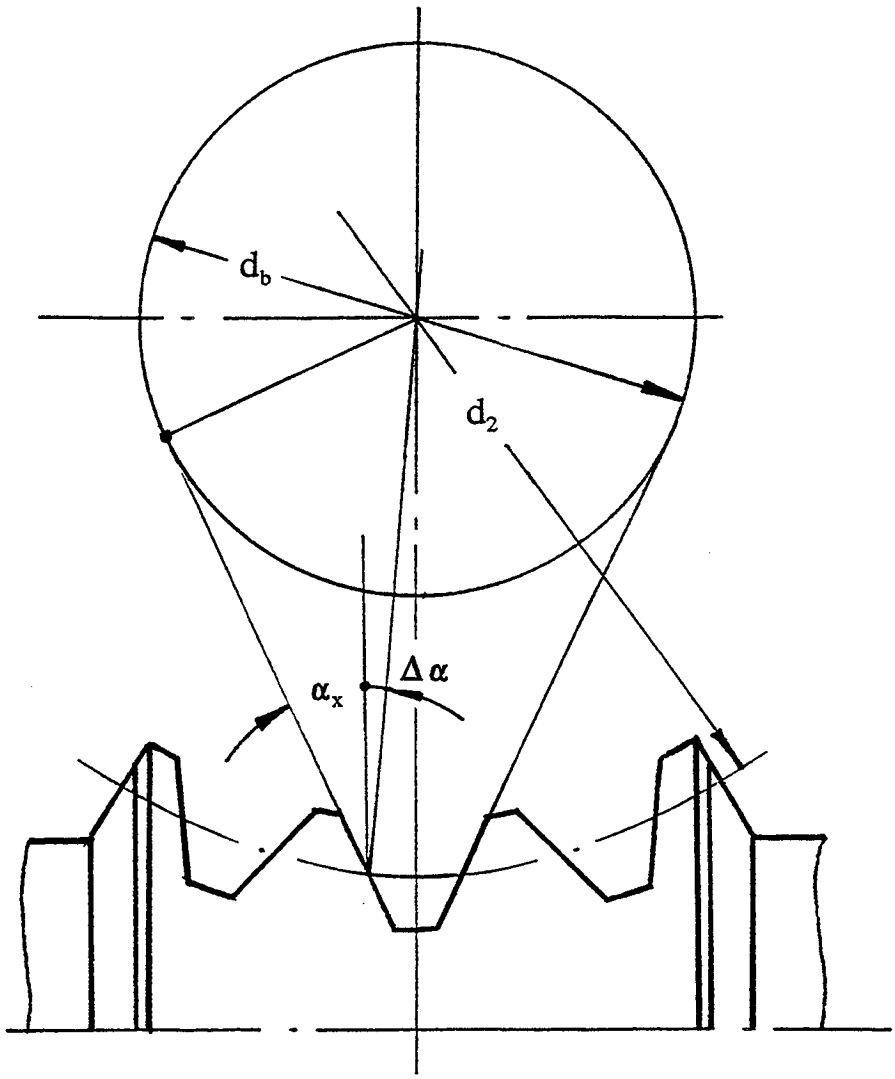

Fig. 1 Symmetric tooth profile

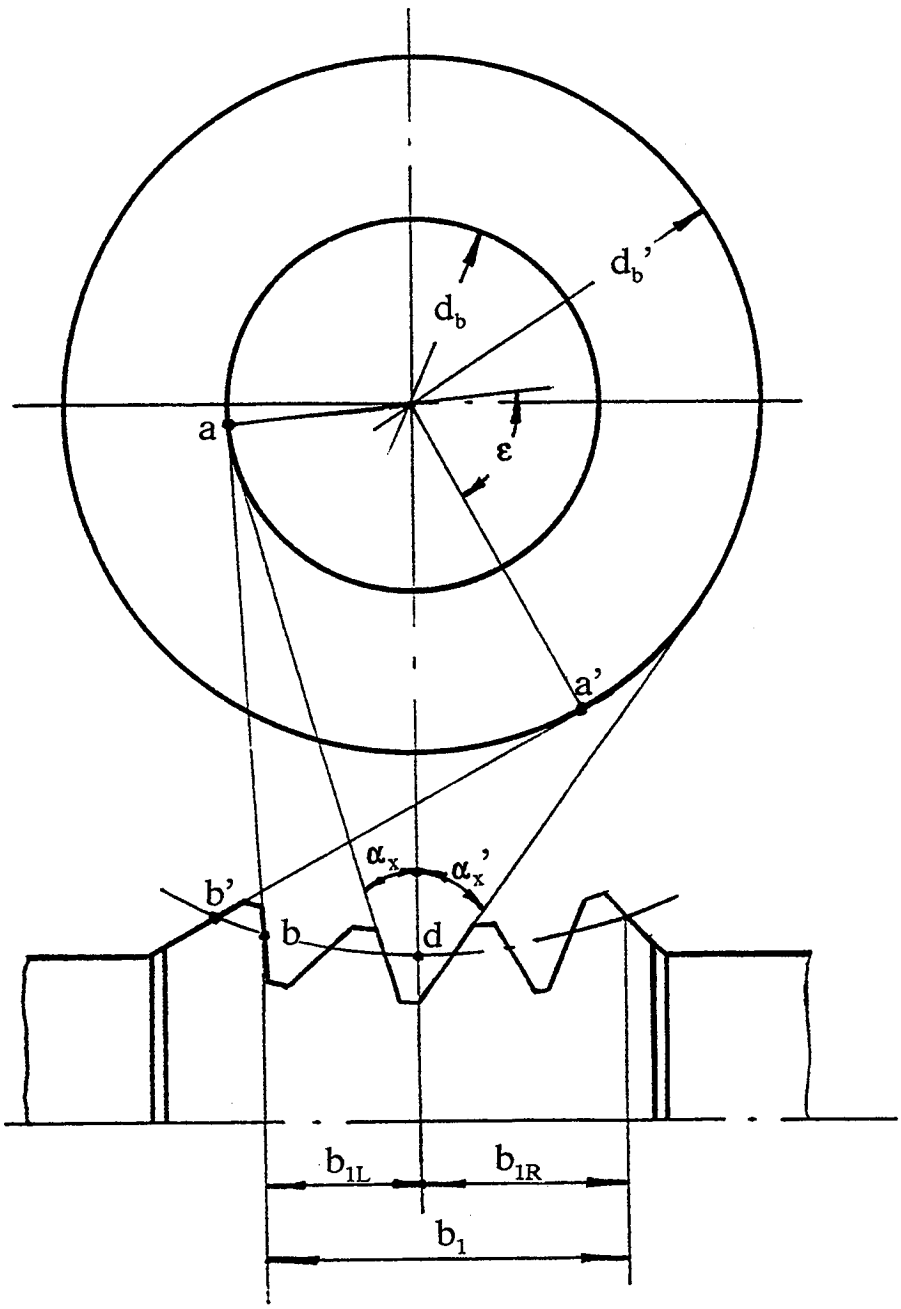

Fig. 2 Non-symmetric tooth profile

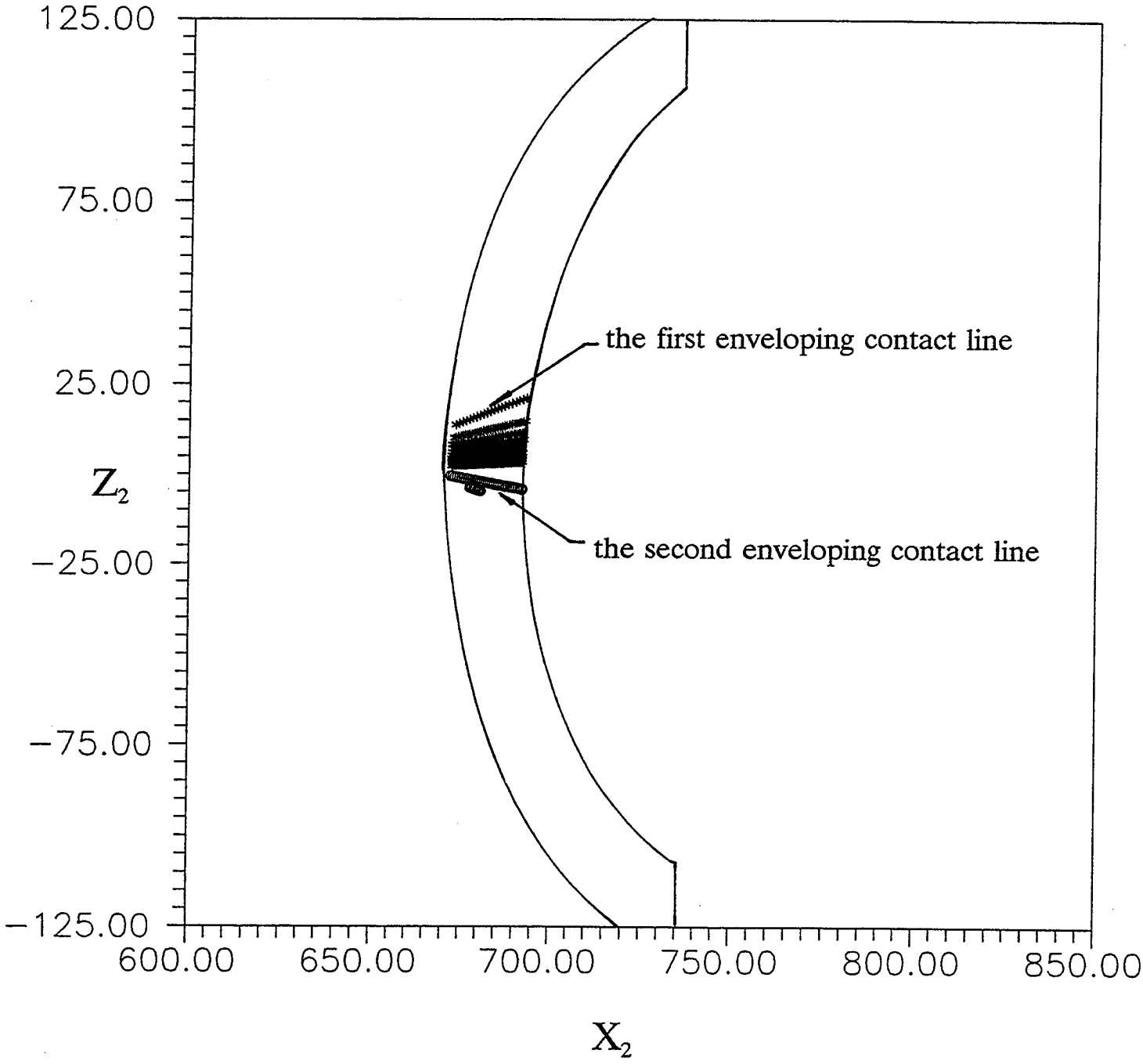

Fig. 3 Distribution of contact lines on a gear tooth
$\alpha_n = 20$ deg, $\beta = 1.5$ deg, $N_p = 10$, $d_1 = 300$ mm

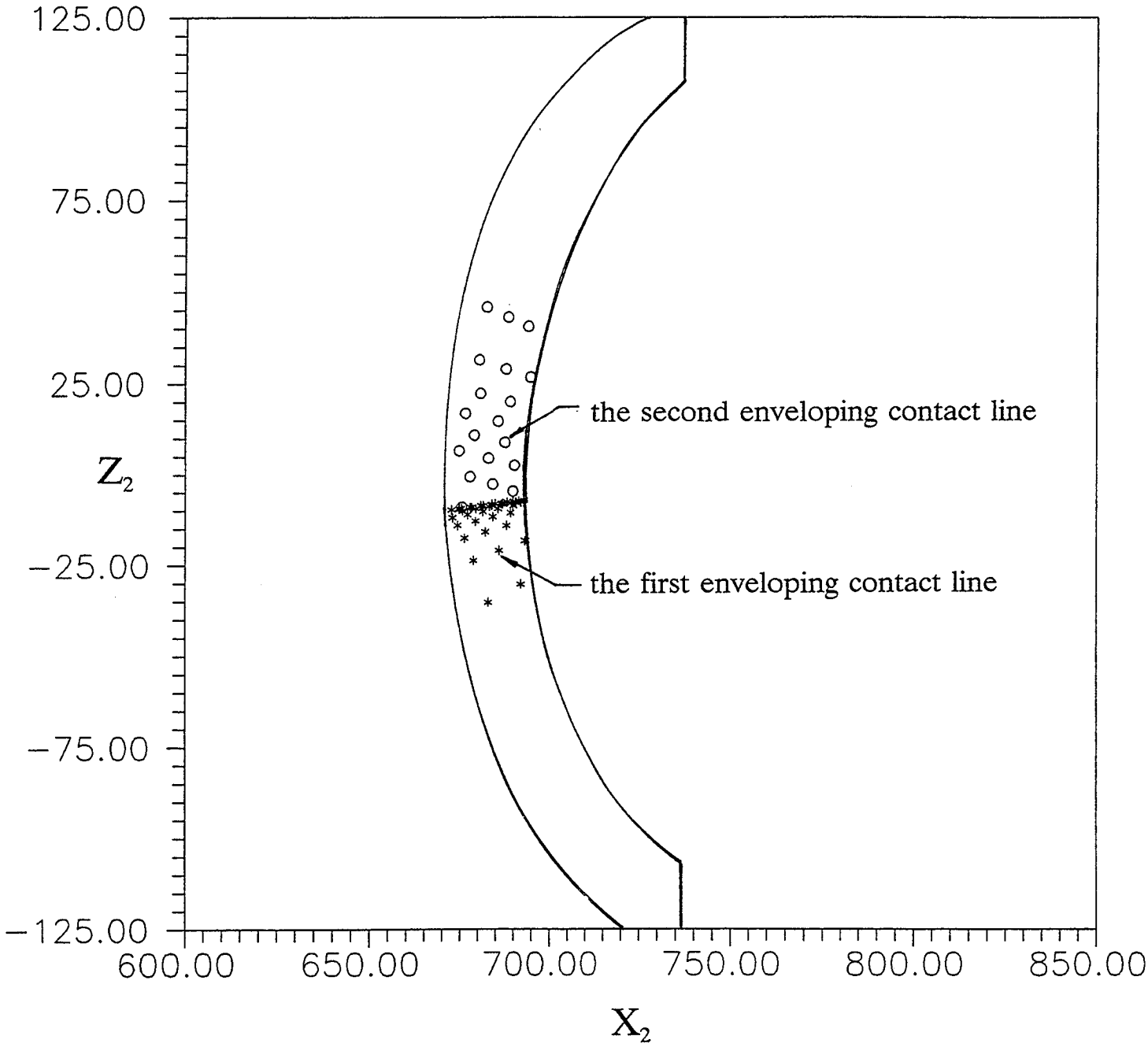

Fig. 4 Distribution of contact lines on a gear tooth
α_n = 20 deg, β = 3.75 deg, N_p = 10, d_1 = 300 mm

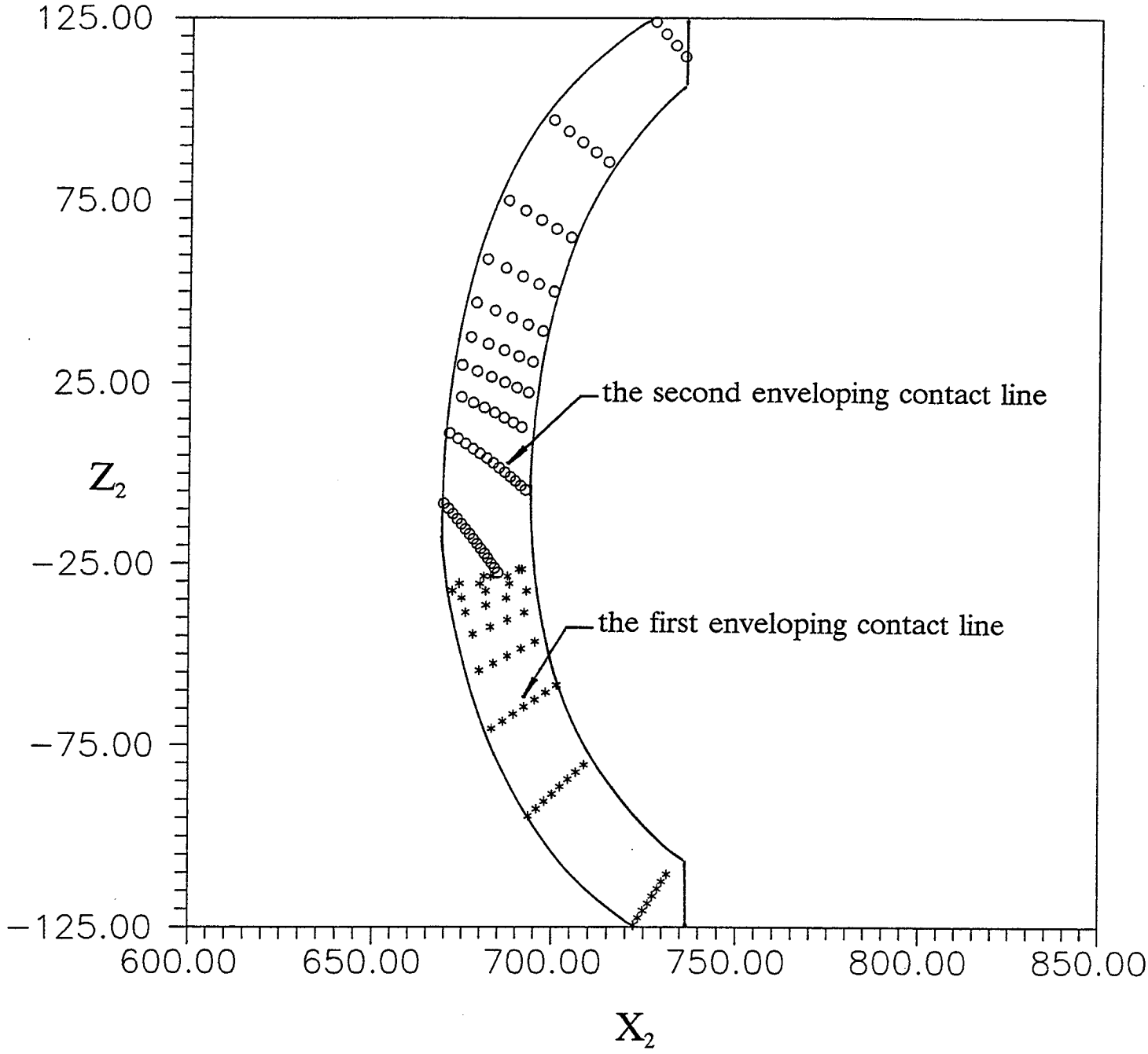

Fig. 5 Distribution of contact lines on a gear tooth
α_n = 20 deg, β = 7.5 deg, N_p = 10, d_1 = 300 mm

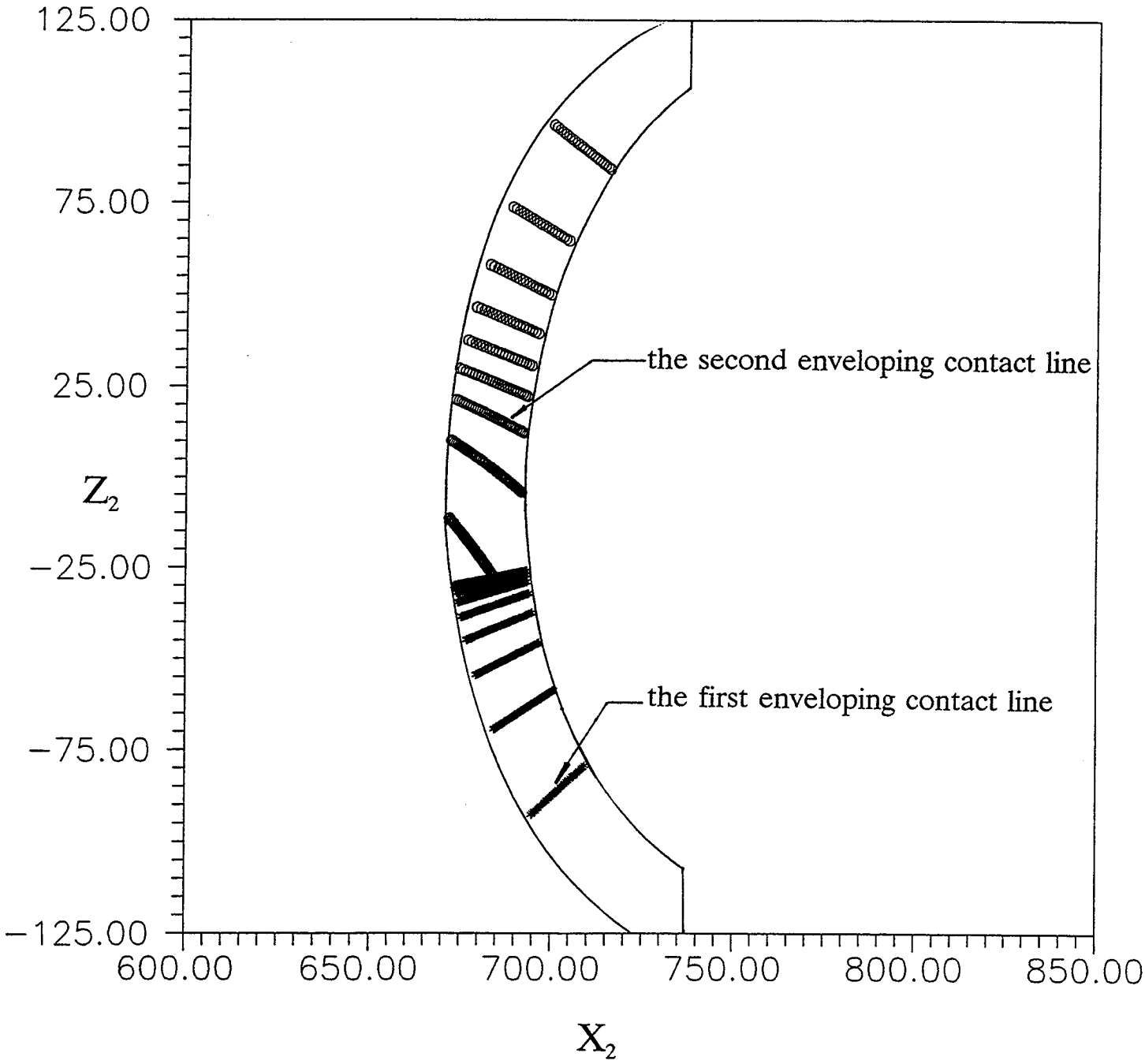

Fig. 6 Distribution of contact lines on a gear tooth
α_n = 20 deg, β = 5 deg, N_p = 10, d_1 = 300 mm

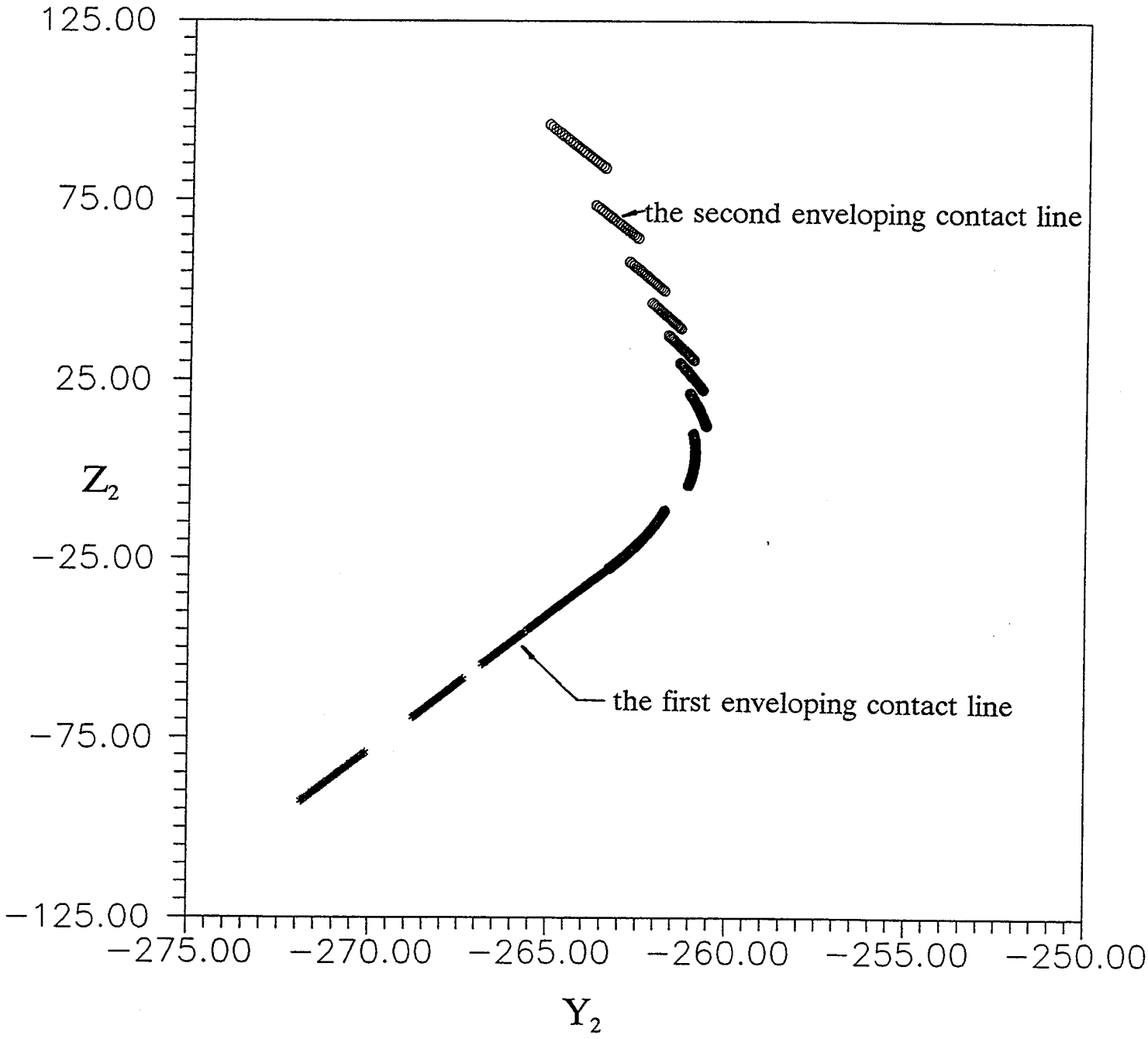

Fig. 7 Distribution of contact lines on a gear tooth
α_n = 20 deg, β = 5 deg, N_p = 10, d_1 = 300 mm

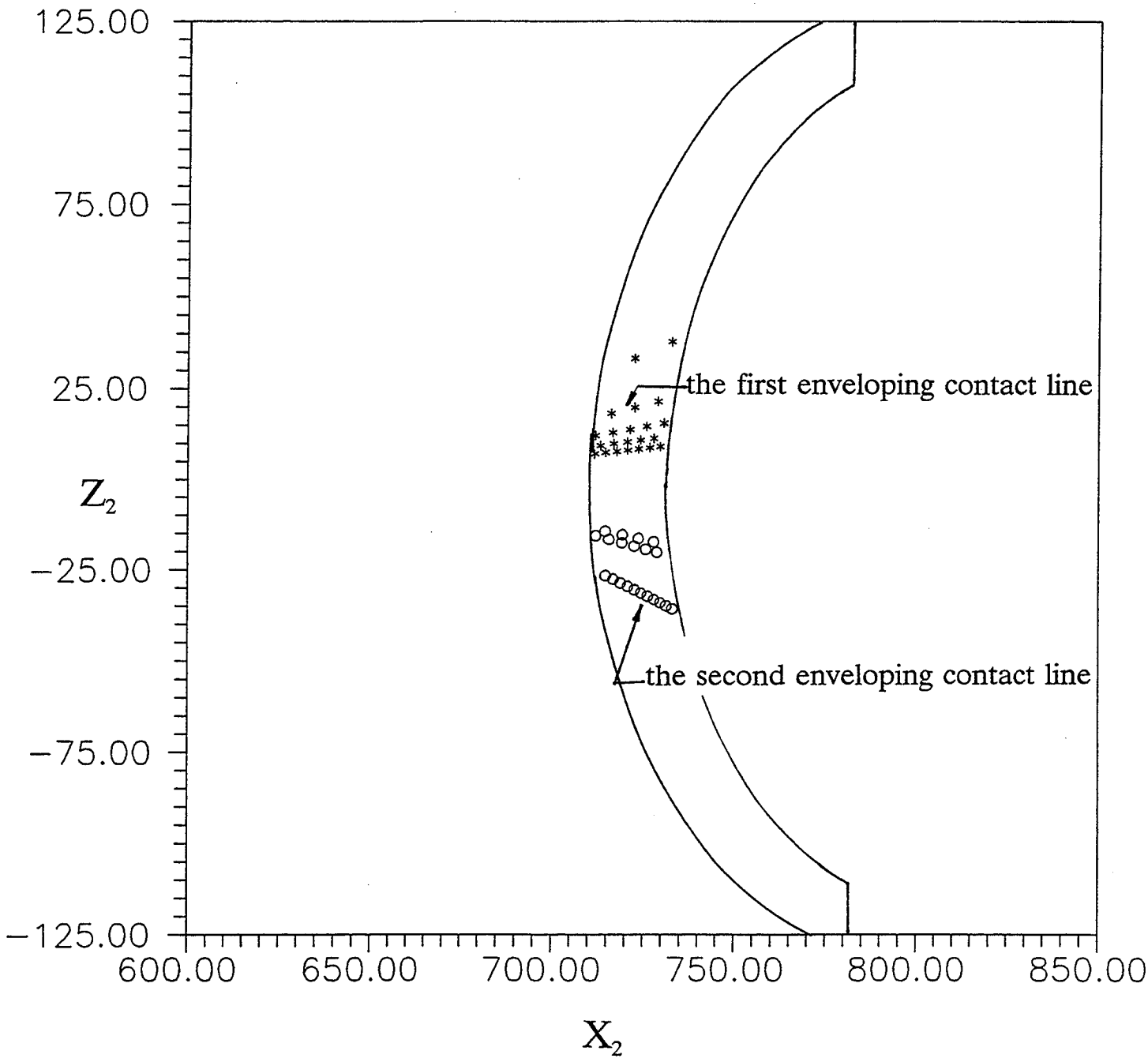

Fig. 8 Distribution of contact lines on a gear tooth
α_n = 8.5 deg, β = 1.5 deg, N_p = 6, d_1 = 300 mm

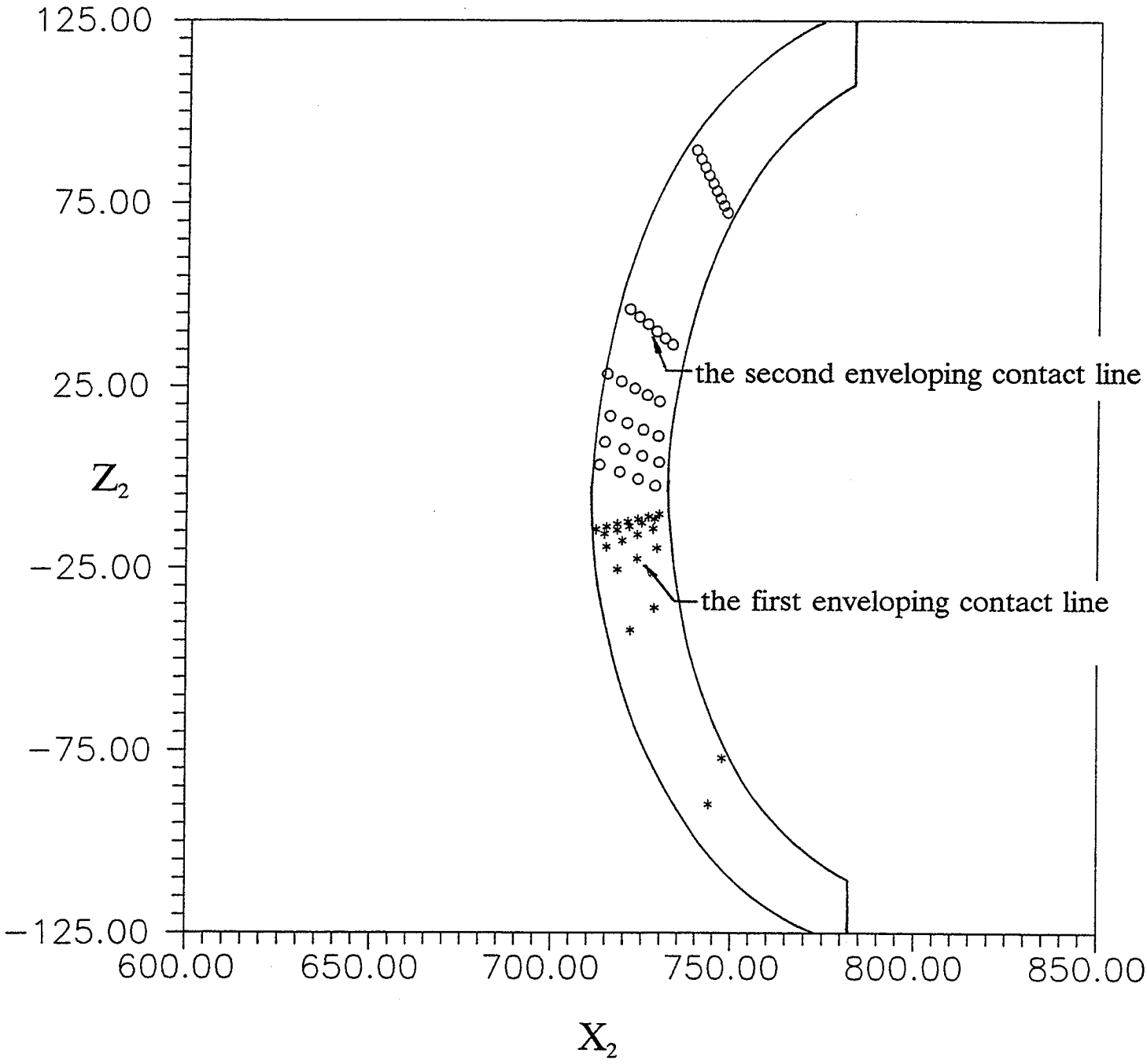

Fig. 9 Distribution of contact lines on a gear tooth
α_n = 8.5 deg, β = 3.75 deg, N_p = 6, d_1 = 300 mm

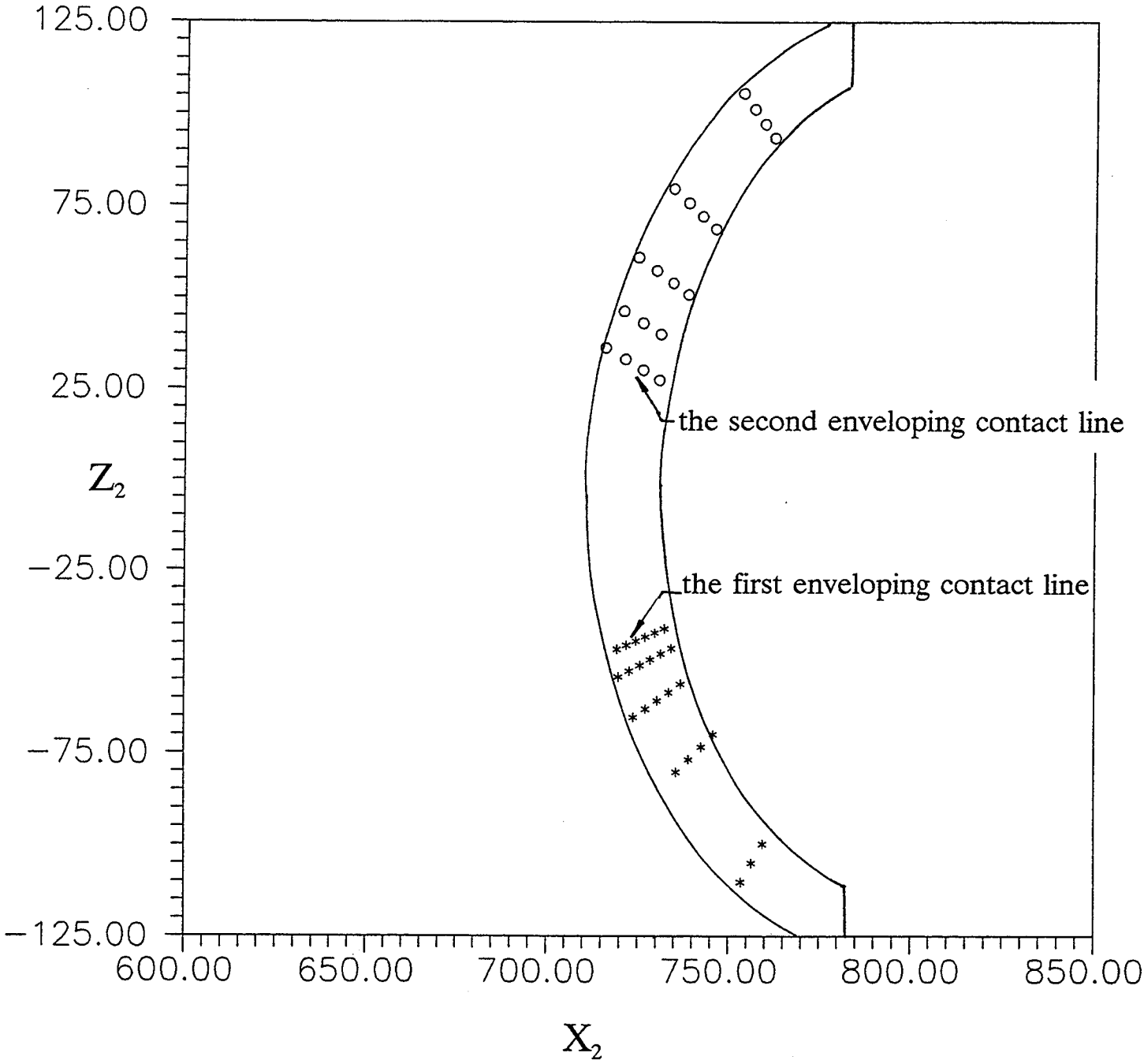

Fig. 10 Distribution of contact lines on a gear tooth
α_n = 8.5 deg, β = 7.5 deg, N_p = 6, d_1 = 300 mm

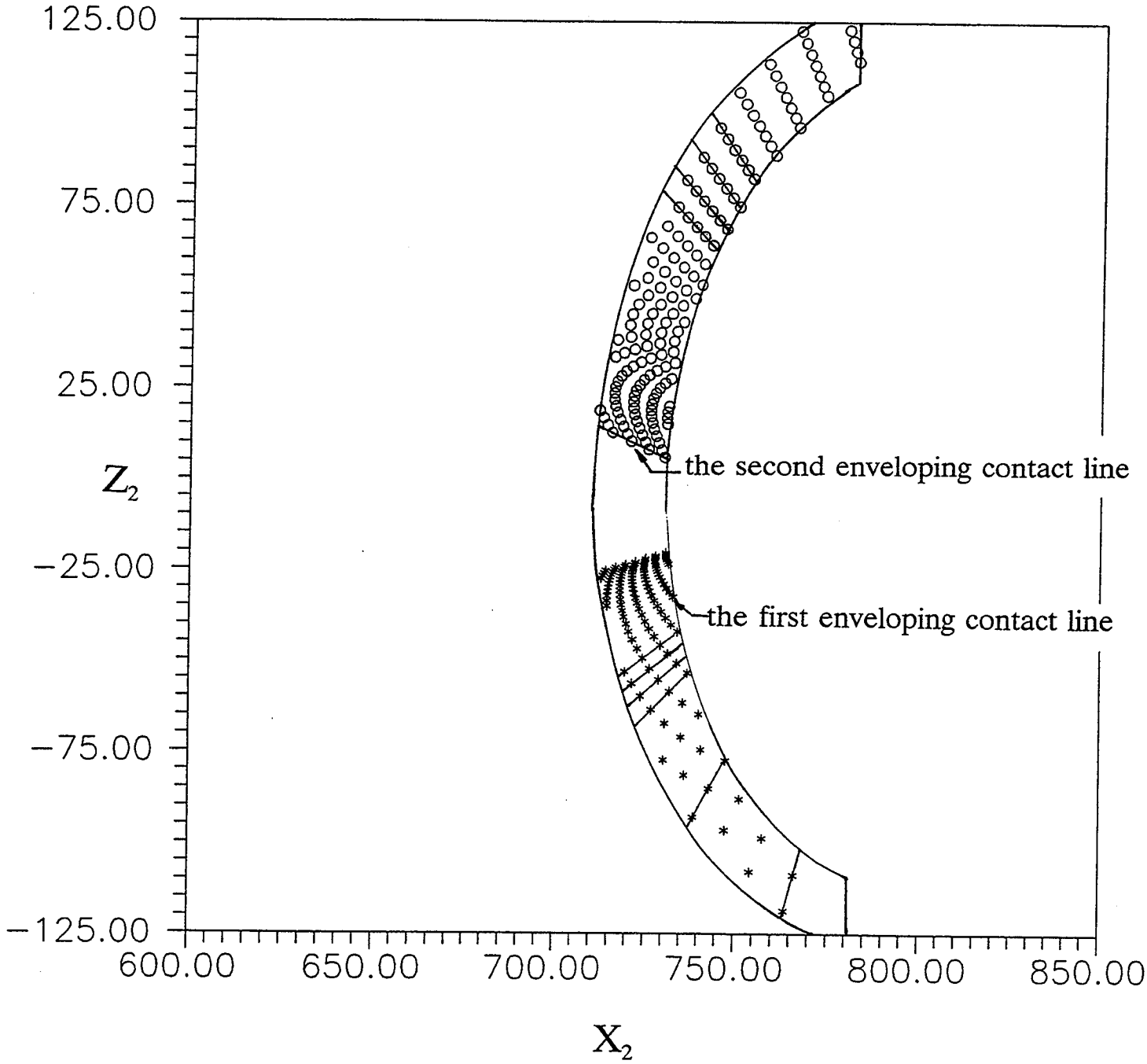

Fig. 11 Distribution of contact lines on a gear tooth
α_n = 8.5 deg, β = 5 deg, N_p = 6, d_1 = 300 mm

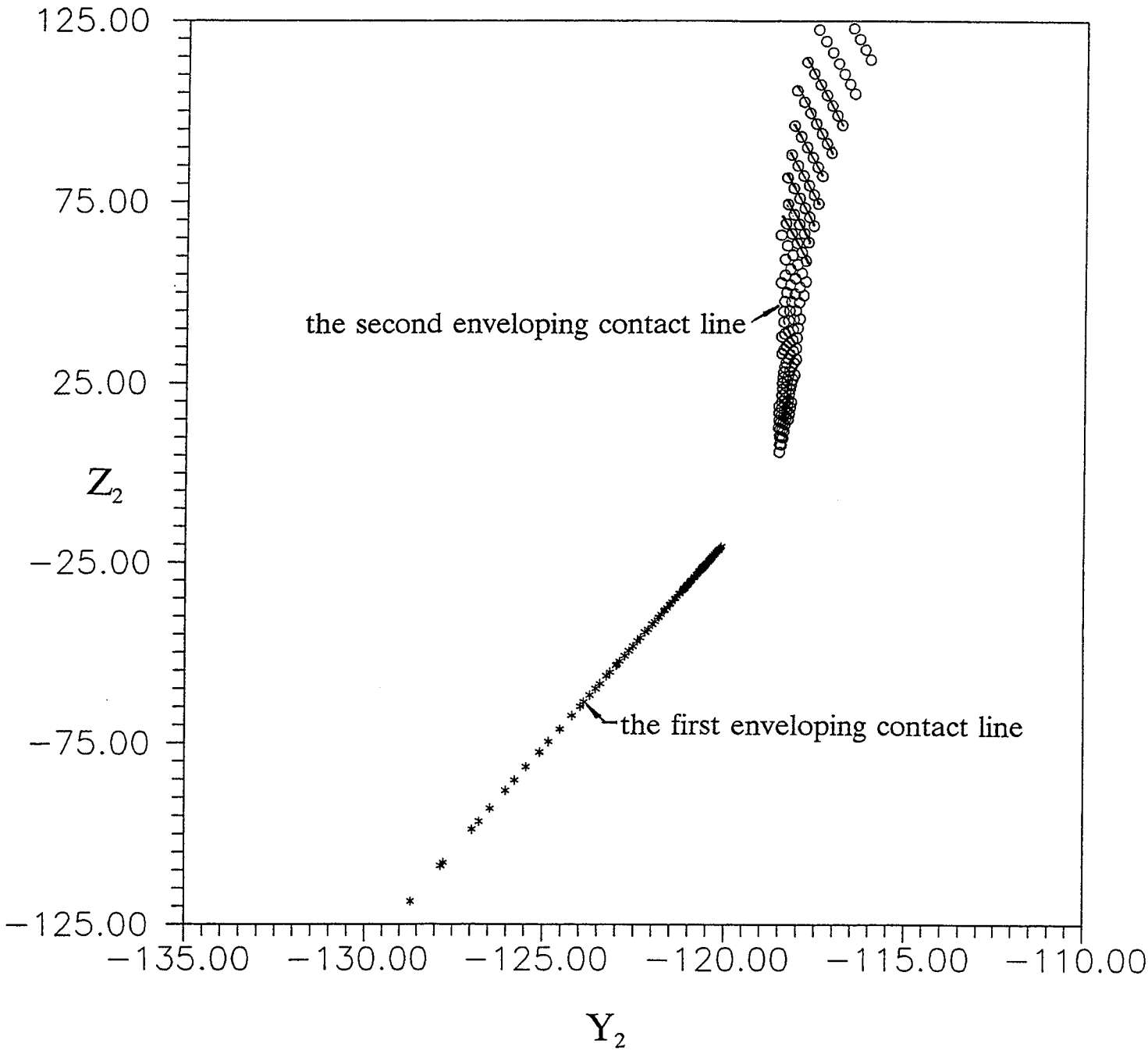

Fig. 12 Distribution of contact lines on a gear tooth
α_n = 8.5 deg, β = 5 deg, N_p = 6, d_1 = 300 mm

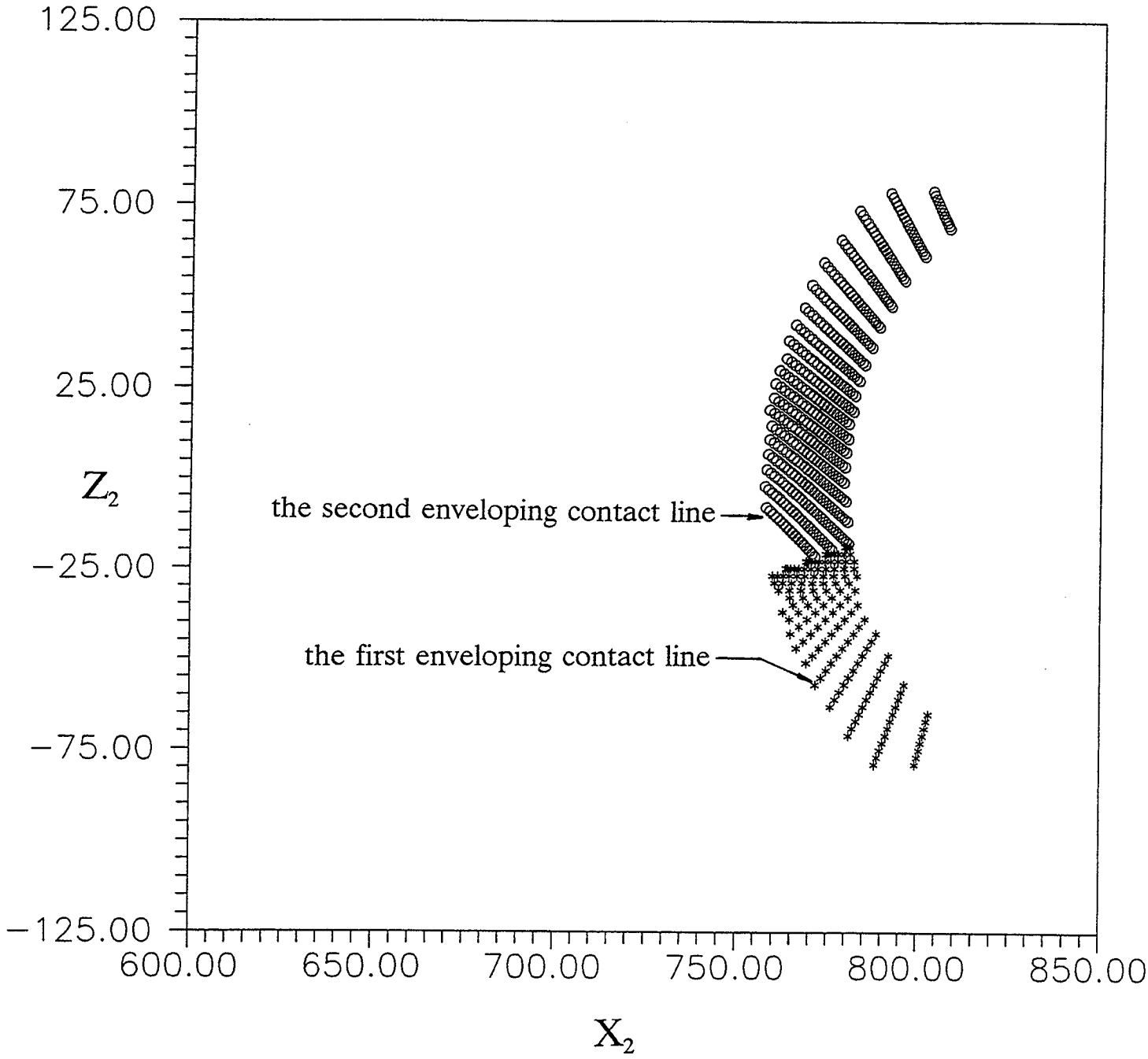

Fig. 13 Distribution of contact lines on a gear tooth
α_n = 8.5 deg, β = 7.5 deg, N_p = 6, d_1 = 200 mm

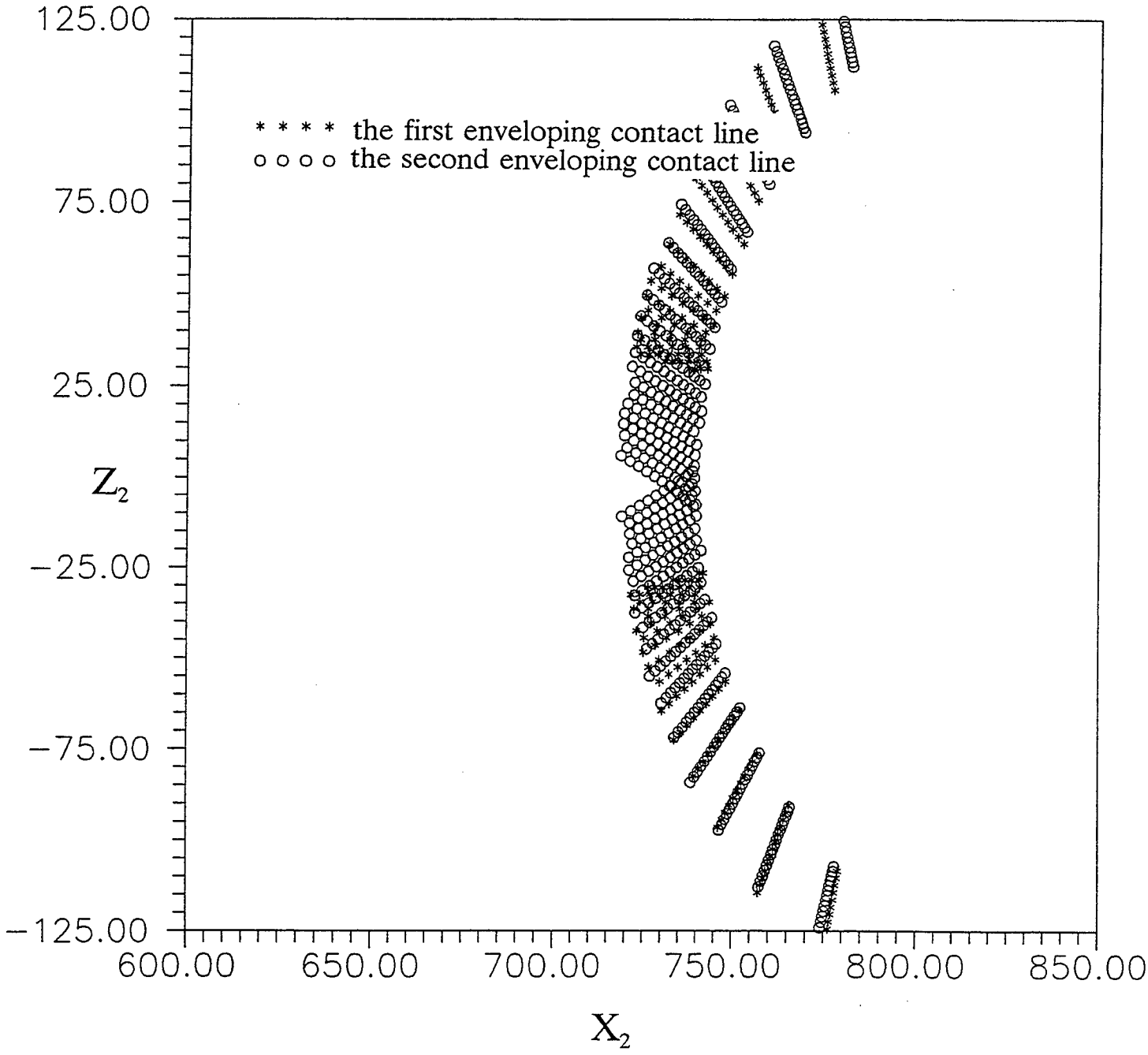

Fig. 14 Distribution of contact lines on a gear tooth
α_n = 0 deg, β = 5 deg, N_p = 10, d_1 = 300 mm

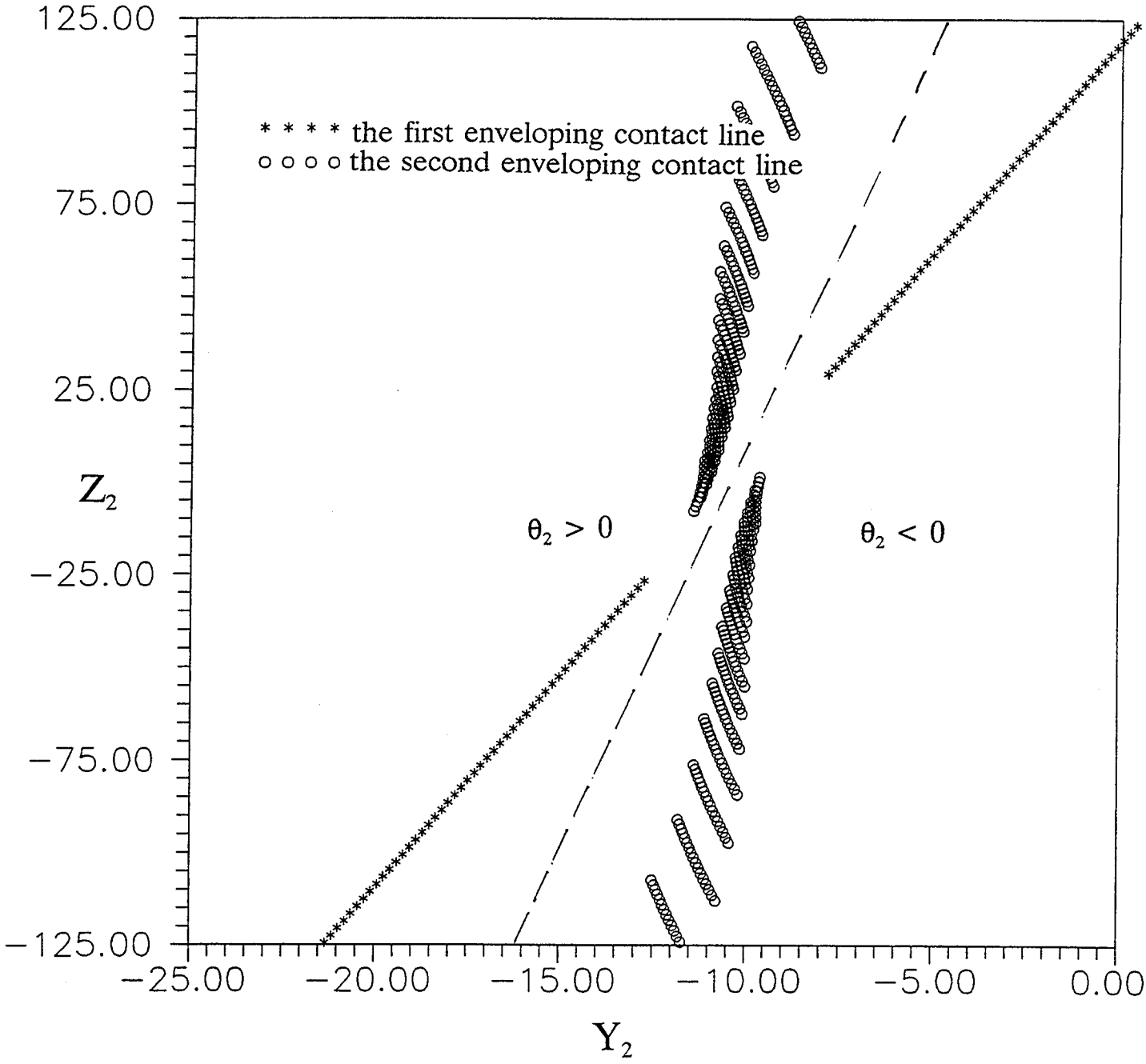

Fig. 15 Distribution of contact lines on a gear tooth
$\alpha_n = 0$ deg, $\beta = 5$ deg, $N_p = 10$, $d_1 = 300$ mm

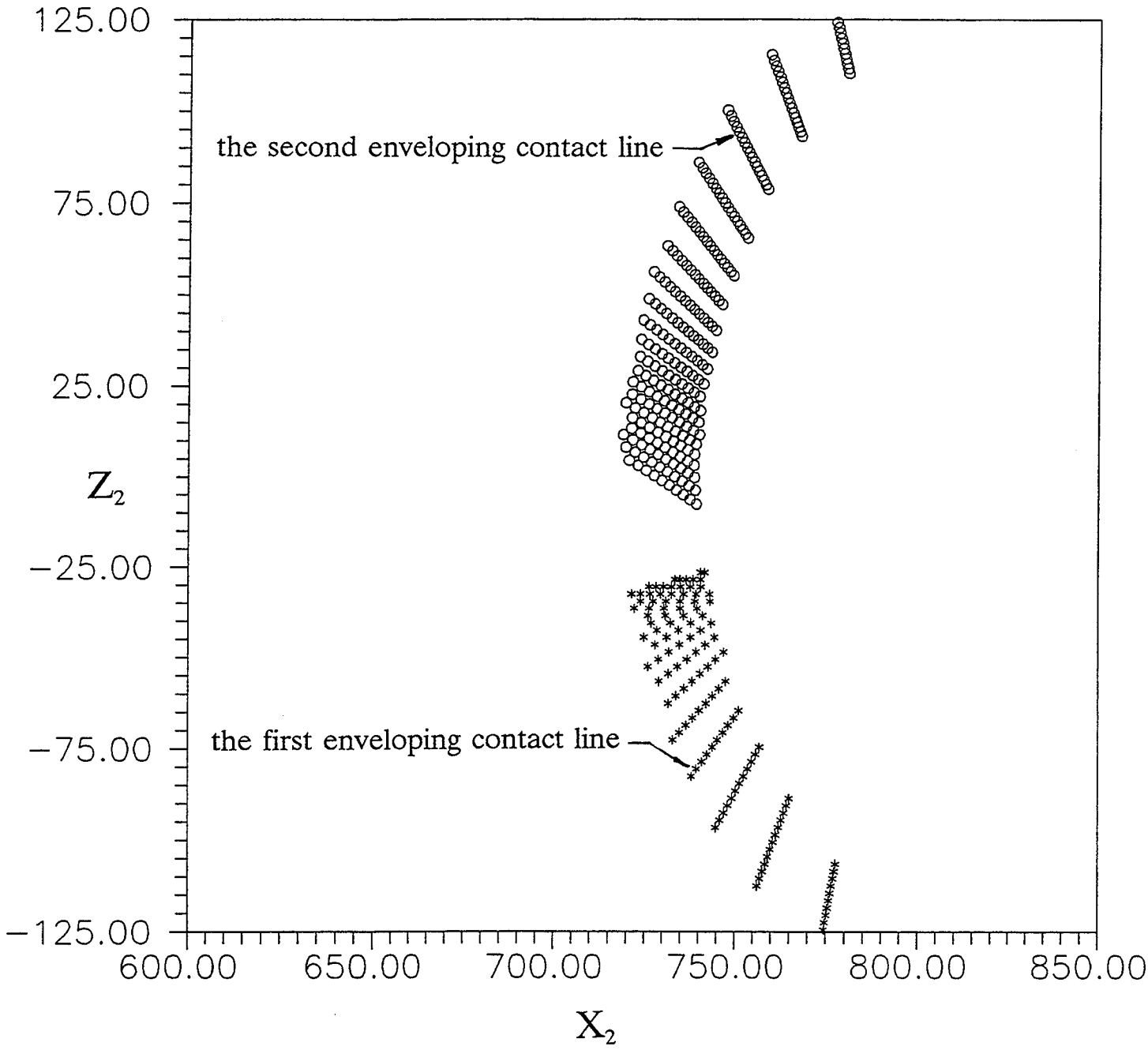

Fig. 16 Distribution of contact lines on a gear tooth
(same parameters as in Fig. 14 except $b_{1L} = 0$)

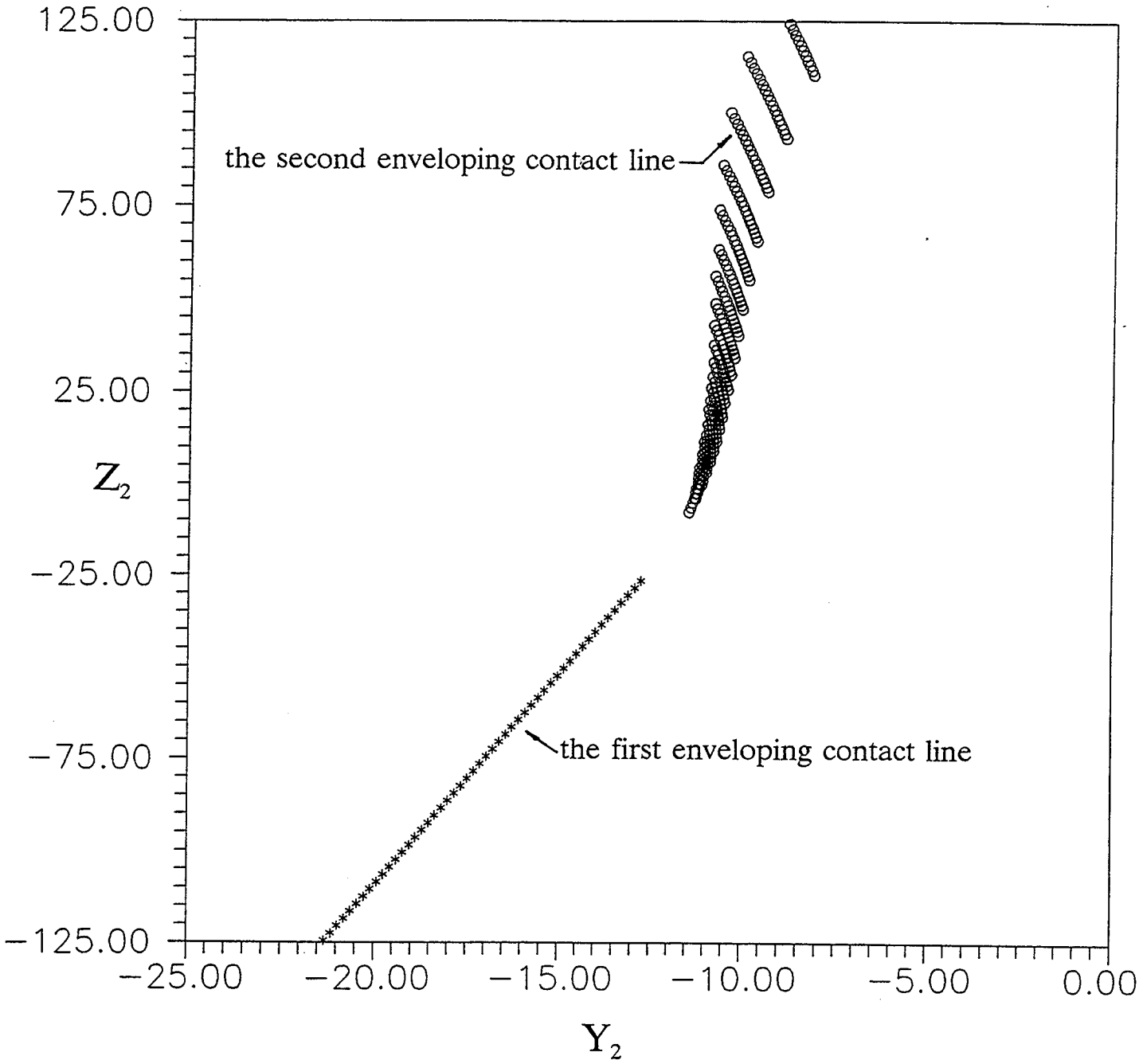

Fig. 17 Distribution of contact lines on a gear tooth
(same parameters as in Fig. 15 except $b_{1L} = 0$)

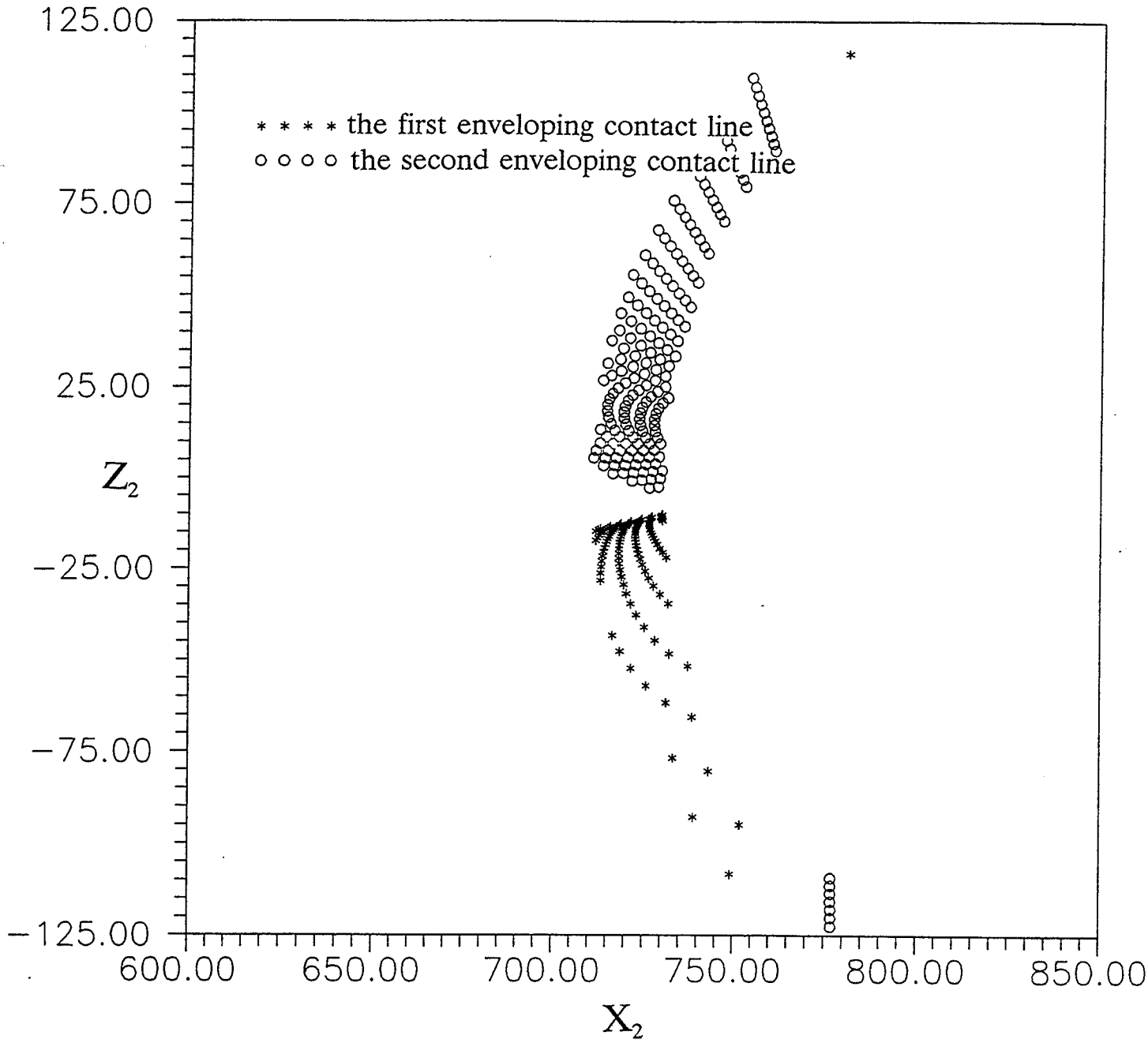

Fig. 18 Distribution of contact lines on a gear tooth
α_n = 8.5 deg, β = 3.5 deg, N_p = 6, d_1 = 300 mm

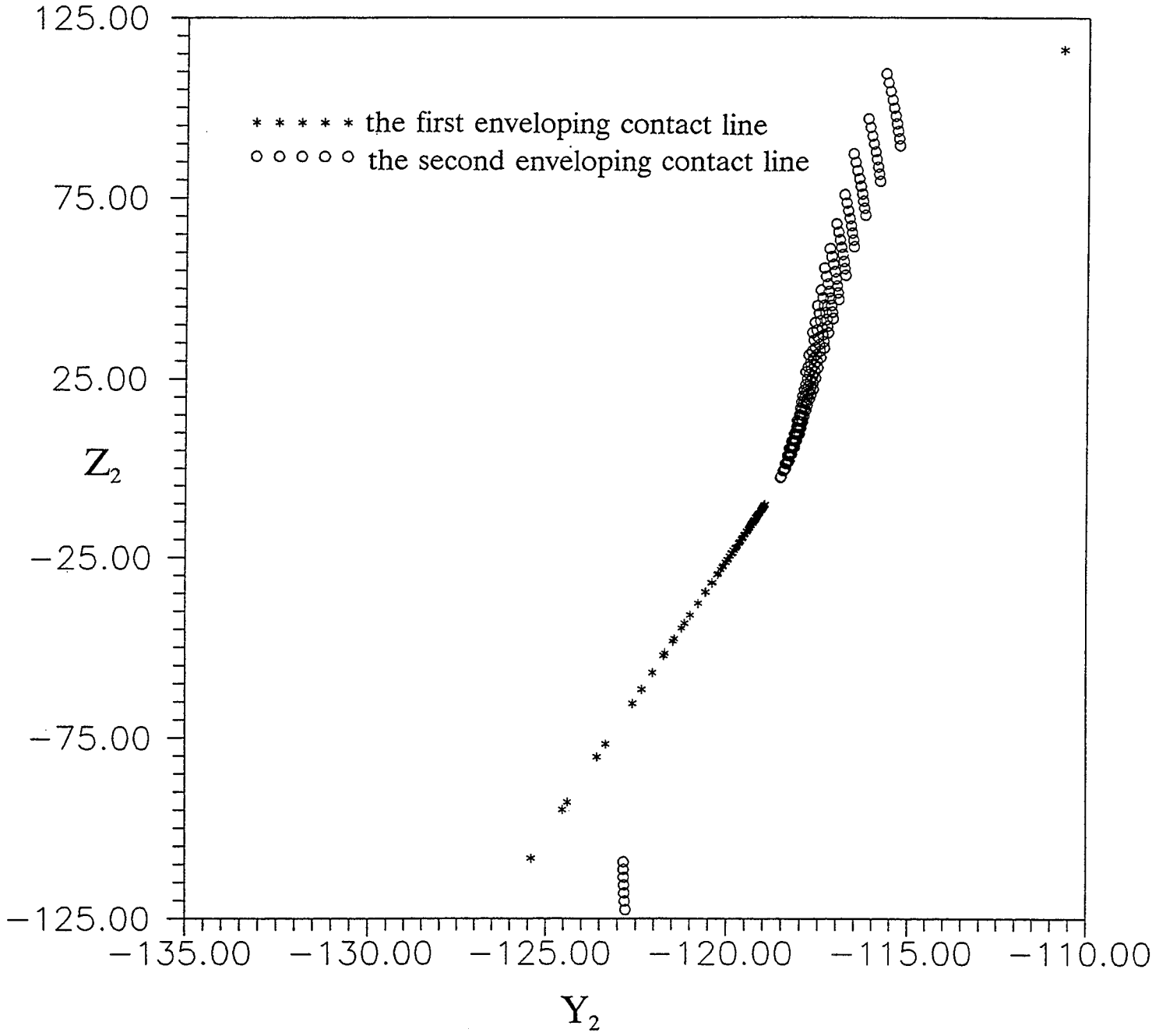

Fig. 19 Distribution of contact lines on a gear tooth
α_n = 8.5 deg, β = 3.5 deg, N_p = 6, d_1 = 300 mm

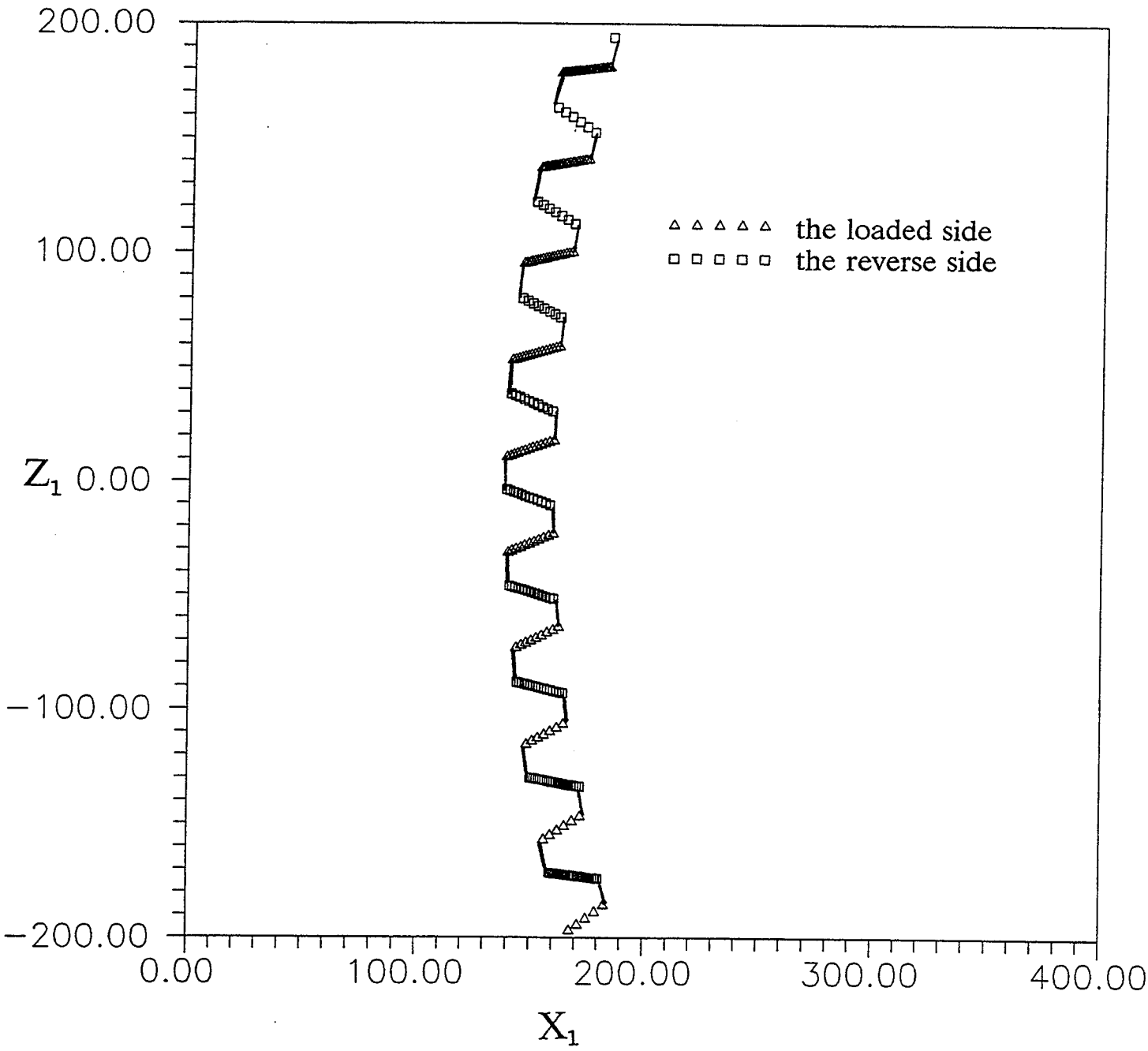

Fig. 20 Worm tooth profile in the mid-plane
α_n = 20 deg, β = 1.5 deg, N_p = 10, d_1 = 300 mm

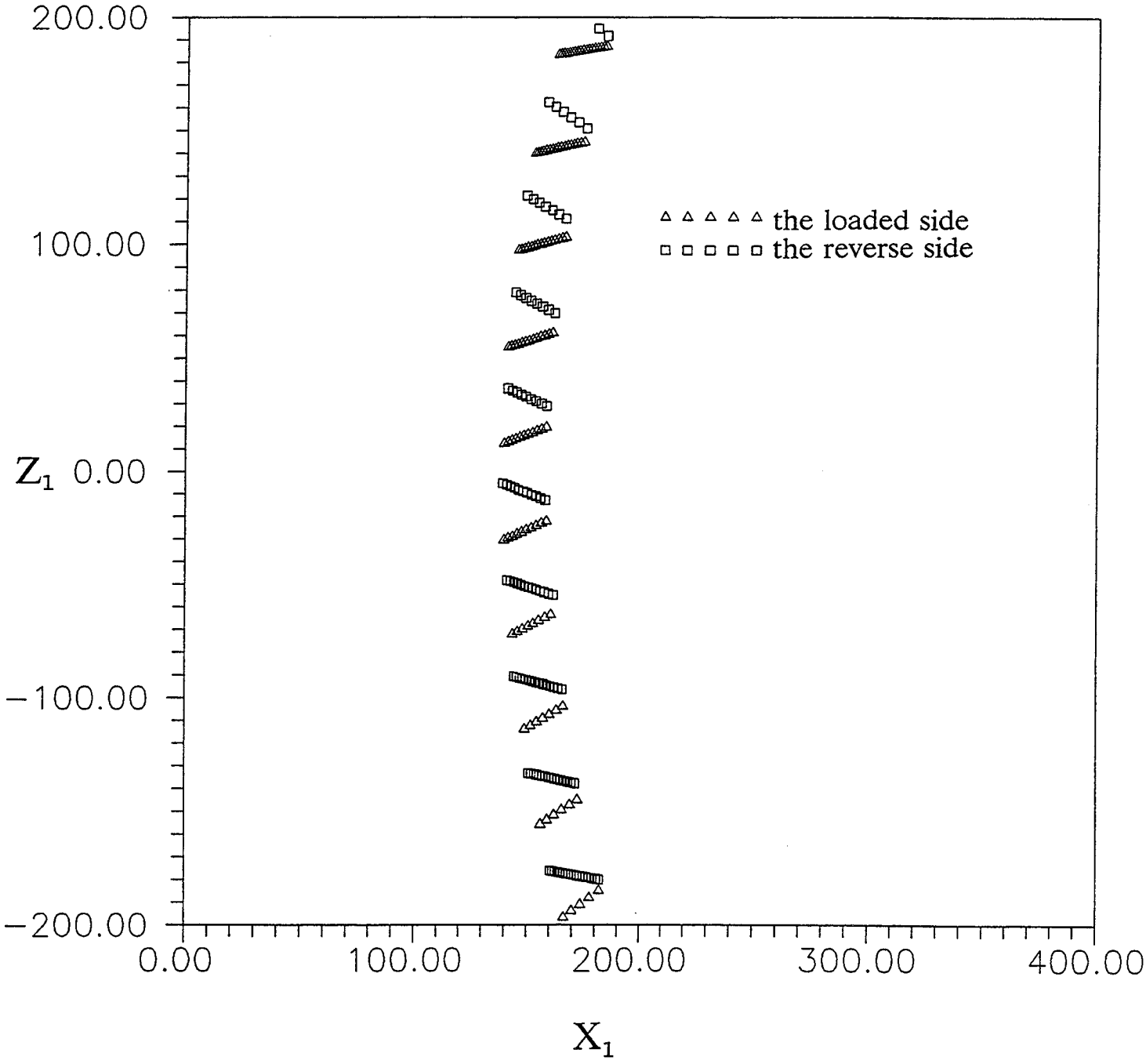

Fig. 21 Worm tooth profile in the mid-plane
α_n = 20 deg, β = 7.5 deg, N_p = 10, d_1 = 300 mm

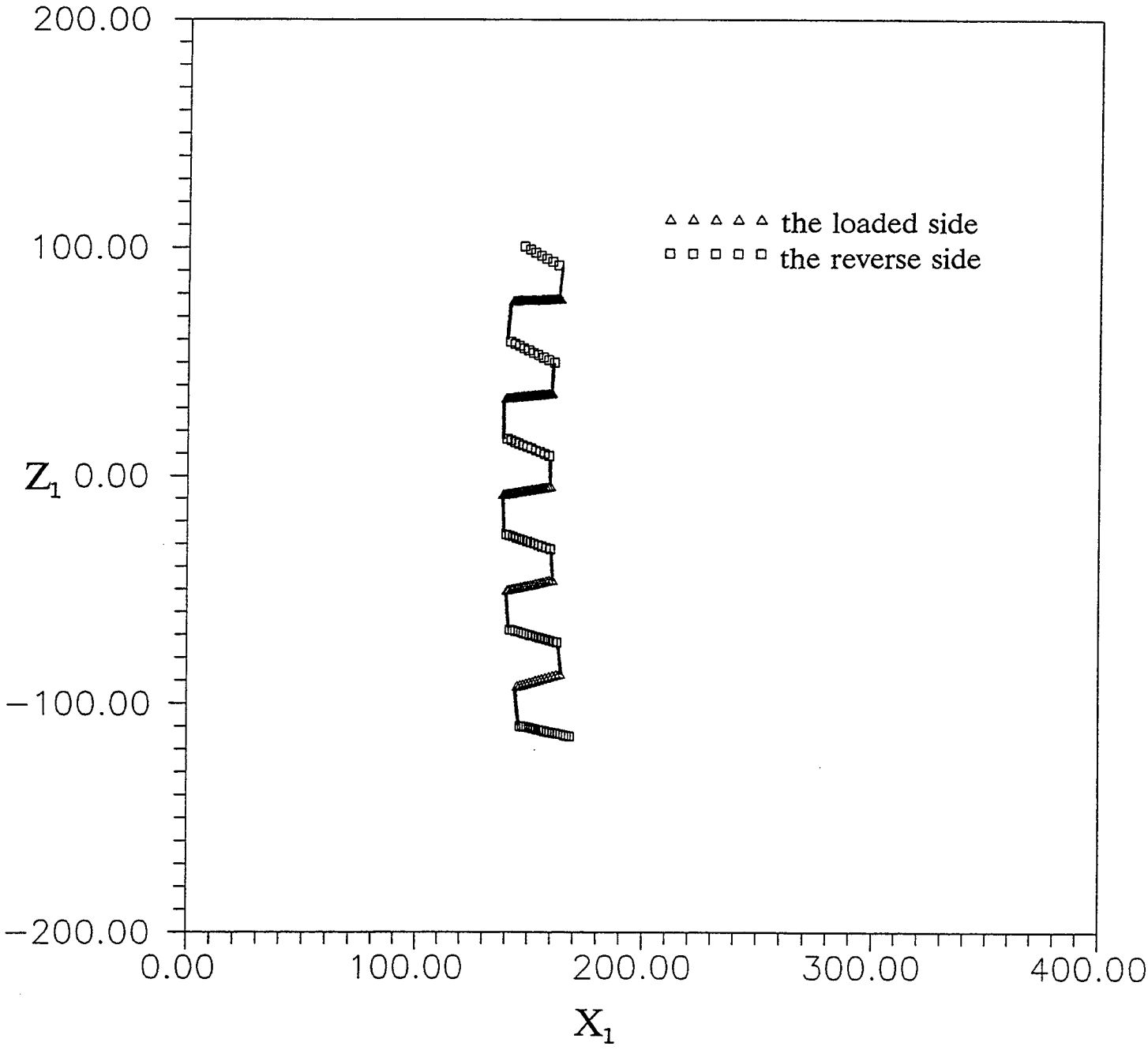

Fig. 22 Worm tooth profile in the mid-plane
α_n = 8.5 deg, β = 1.5 deg, N_p = 6, d_1 = 300 mm

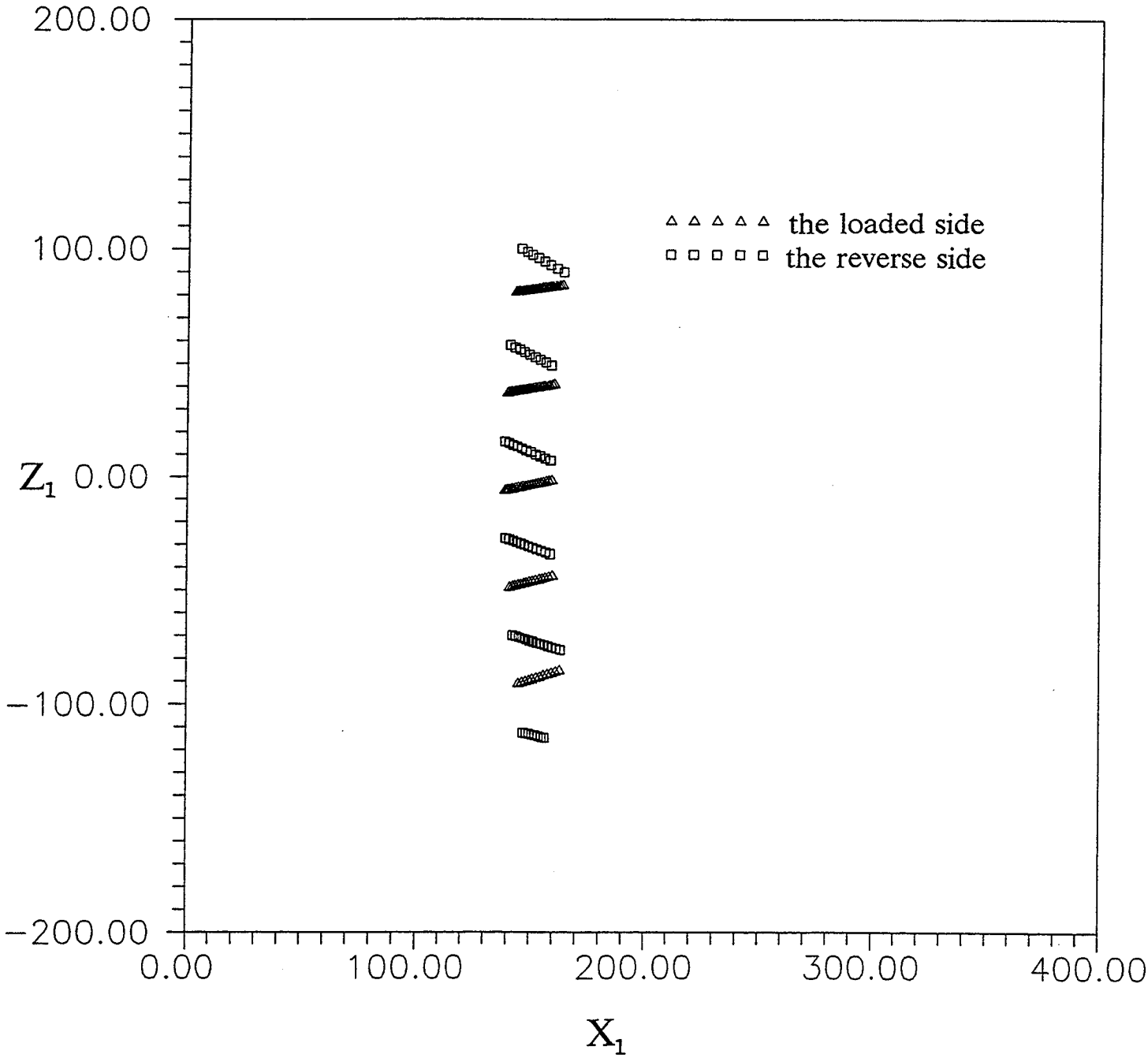

Fig. 23 Worm tooth profile in the mid-plane
α_n = 8.5 deg, β = 7.5 deg, N_p = 6, d_1 = 300 mm

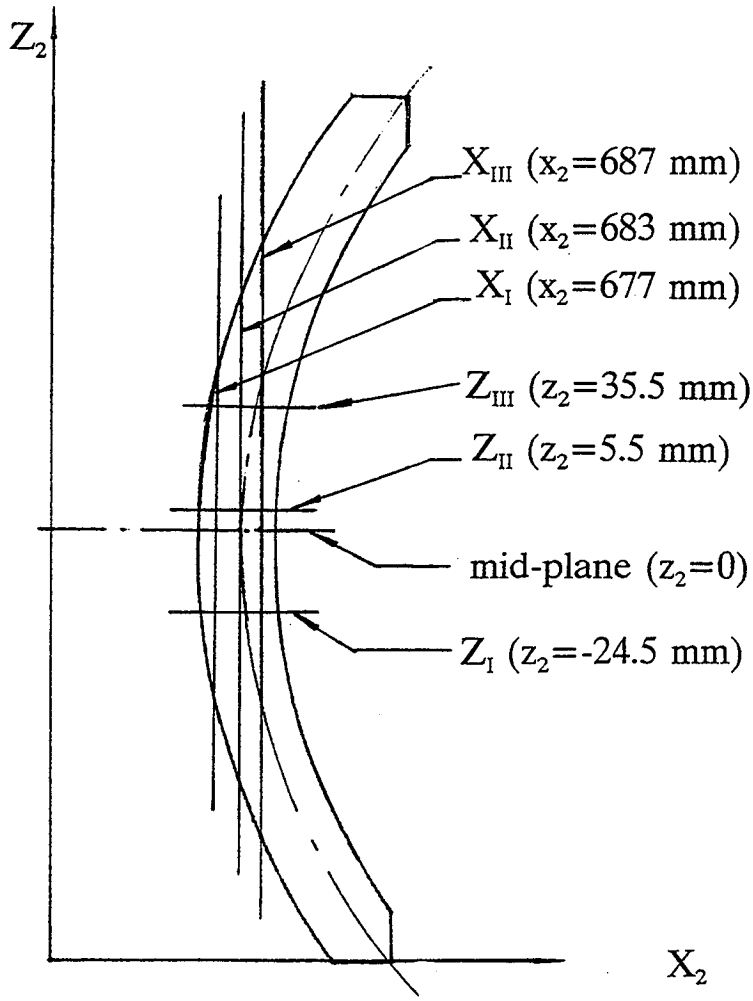

Fig. 24 Sections where the clearance function is shown

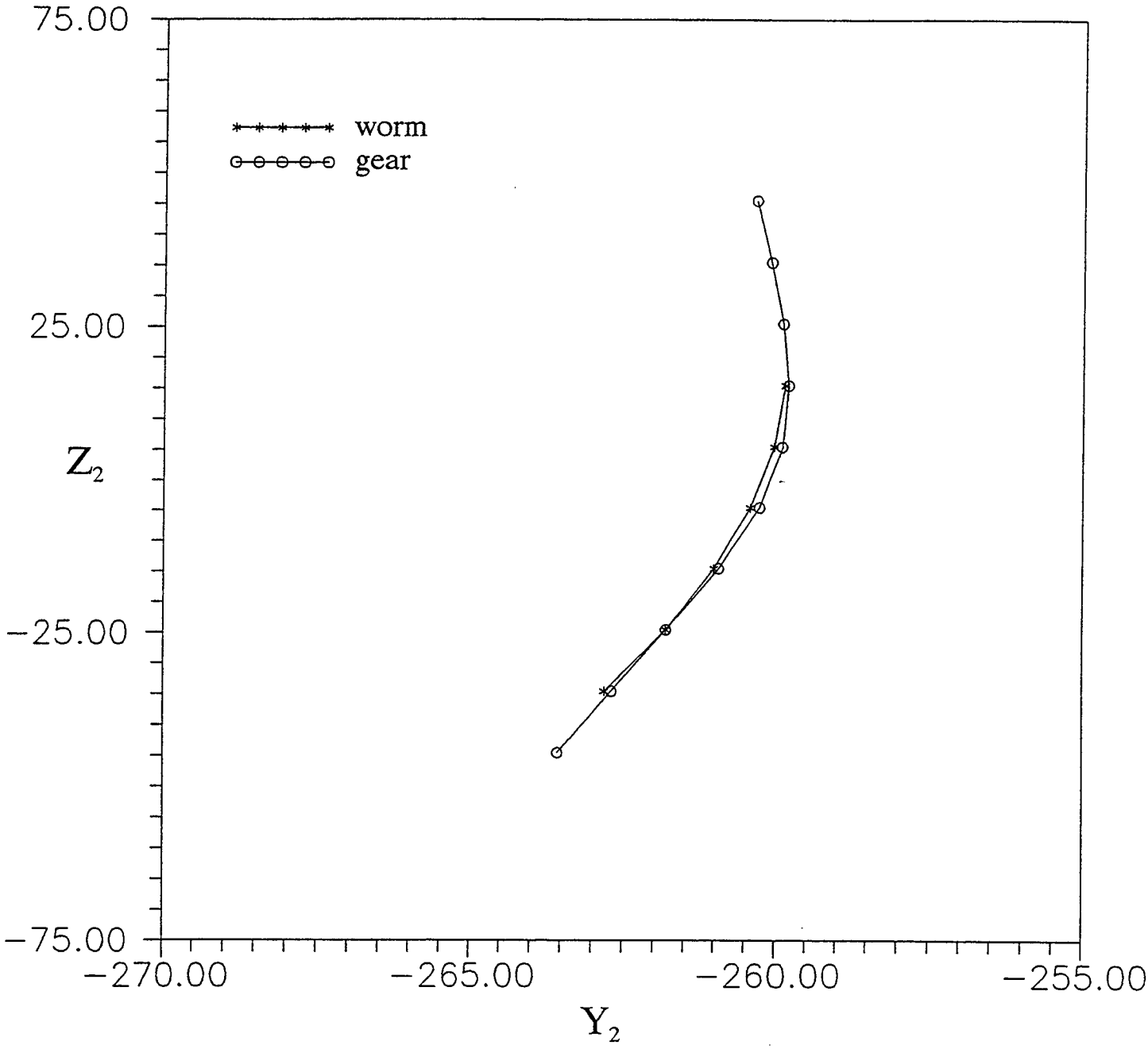

Fig. 25 Clearance function at x_i (α_n = 20 deg)

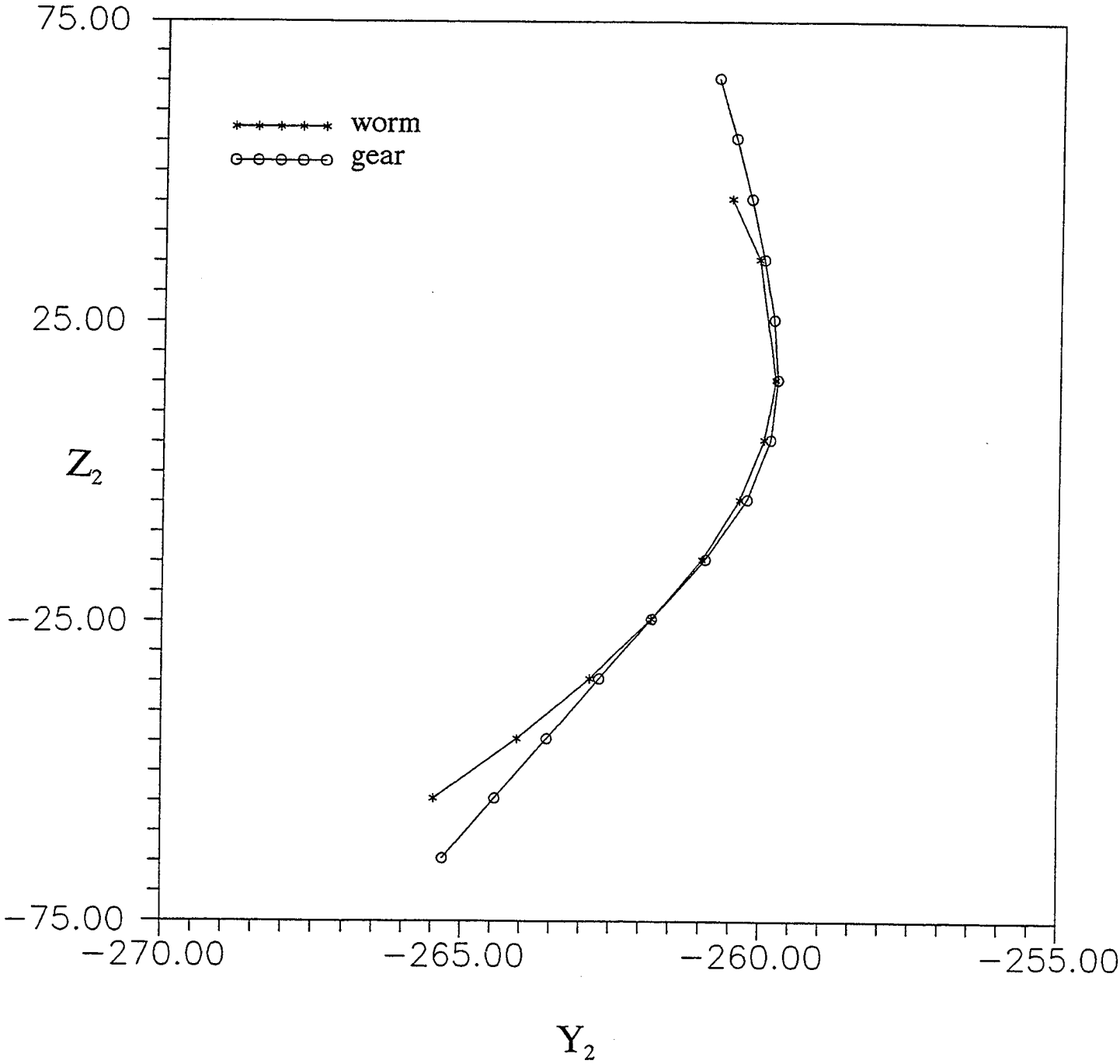

Fig. 26 Clearance function at x_{II} (α_n = 20 deg)

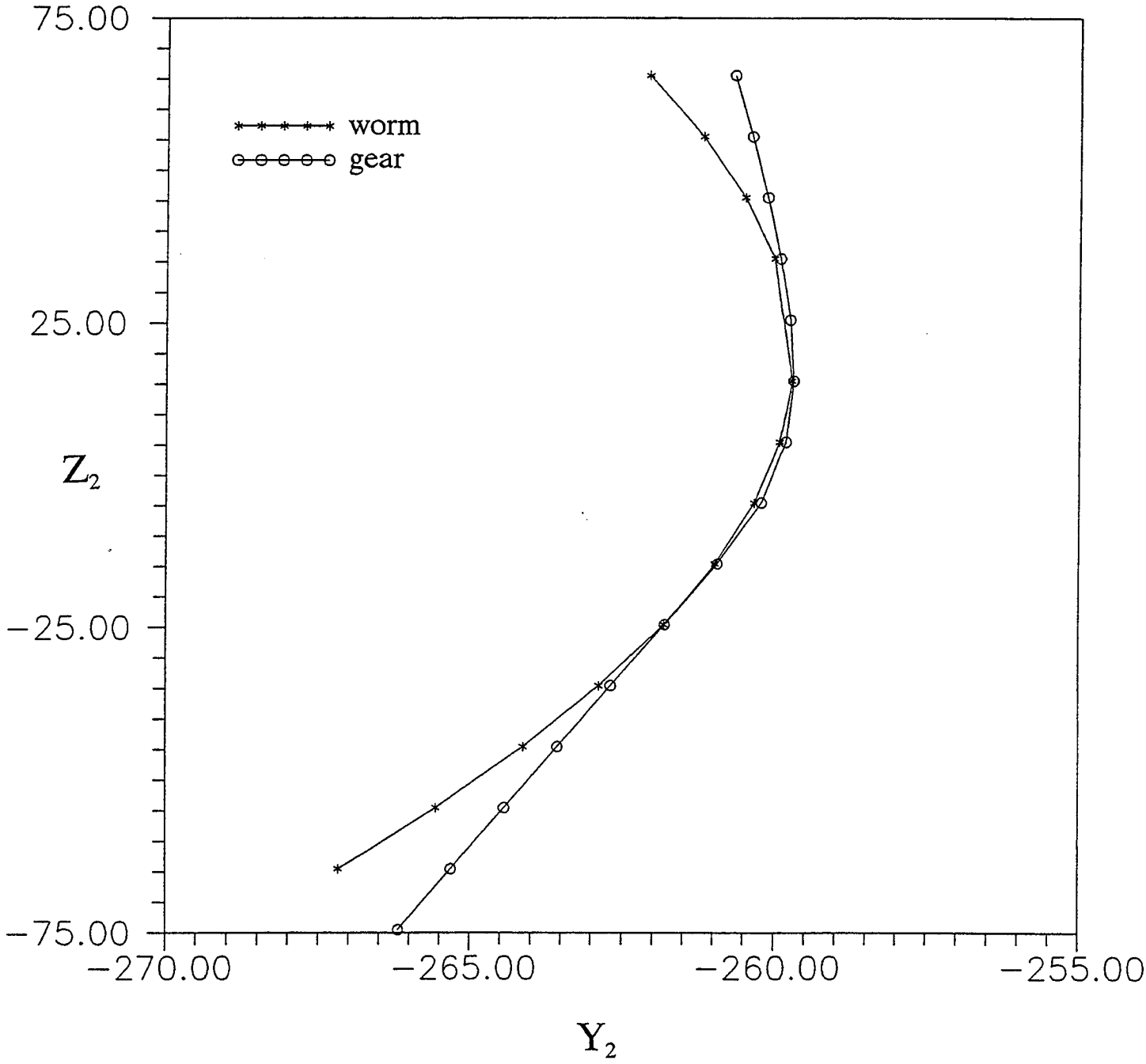

Fig. 27 Clearance function at x_{III} (α_n = 20 deg)

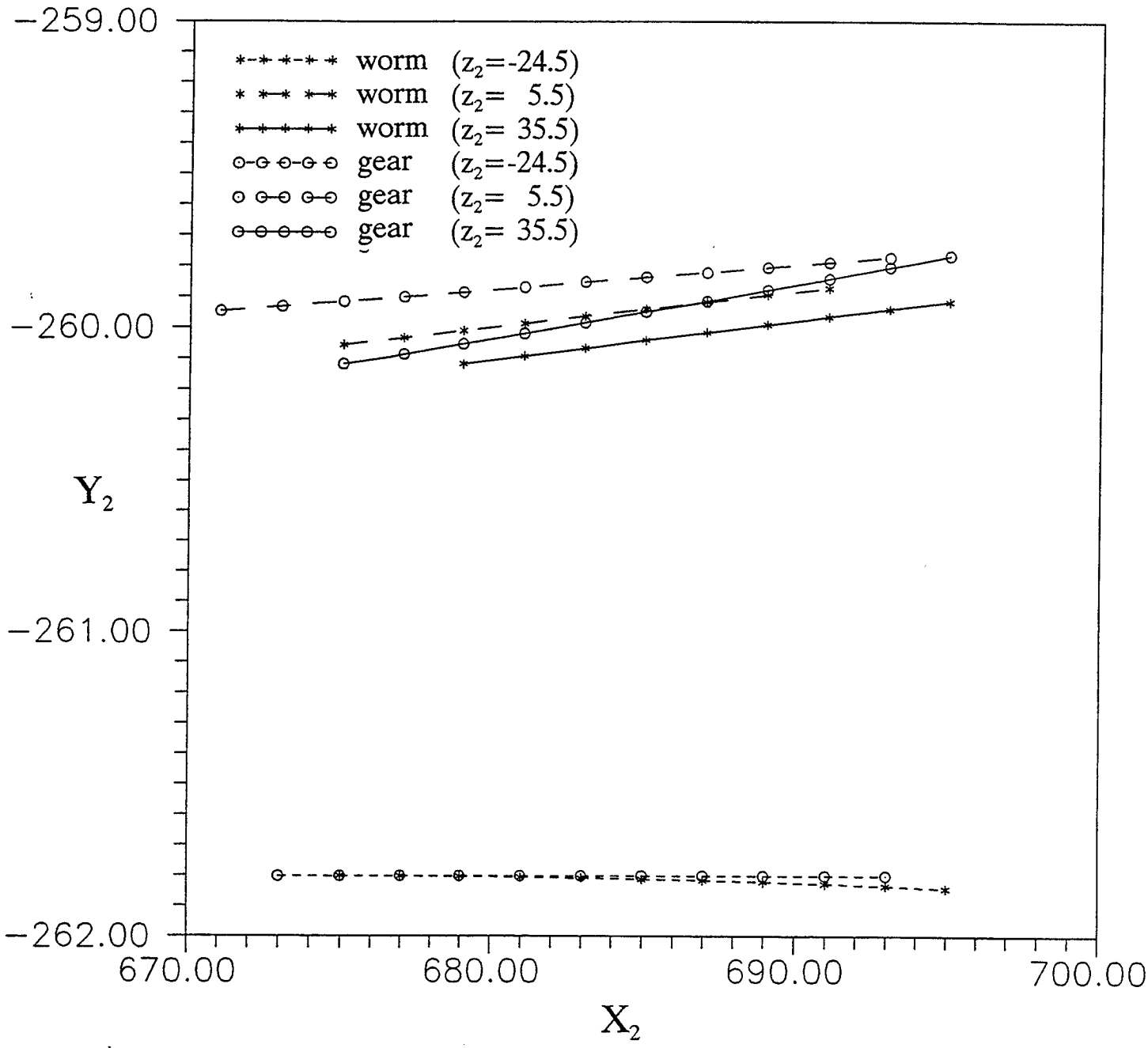

Fig. 28 Clearance function at z_I, z_{II} and z_{III} (α_n = 20 deg)

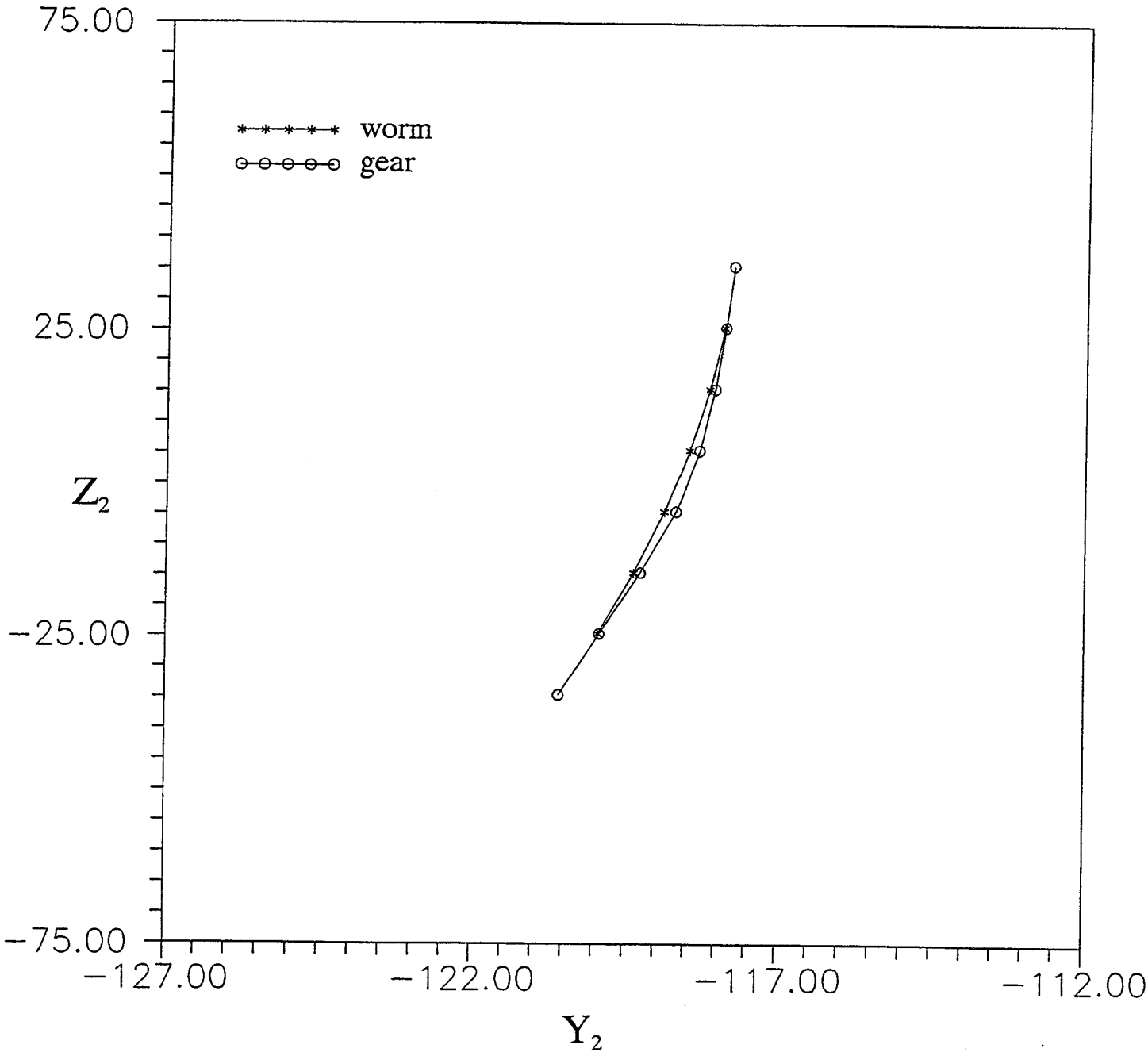

Fig. 29 Clearance function at x_1 (α_n = 8.5 deg)

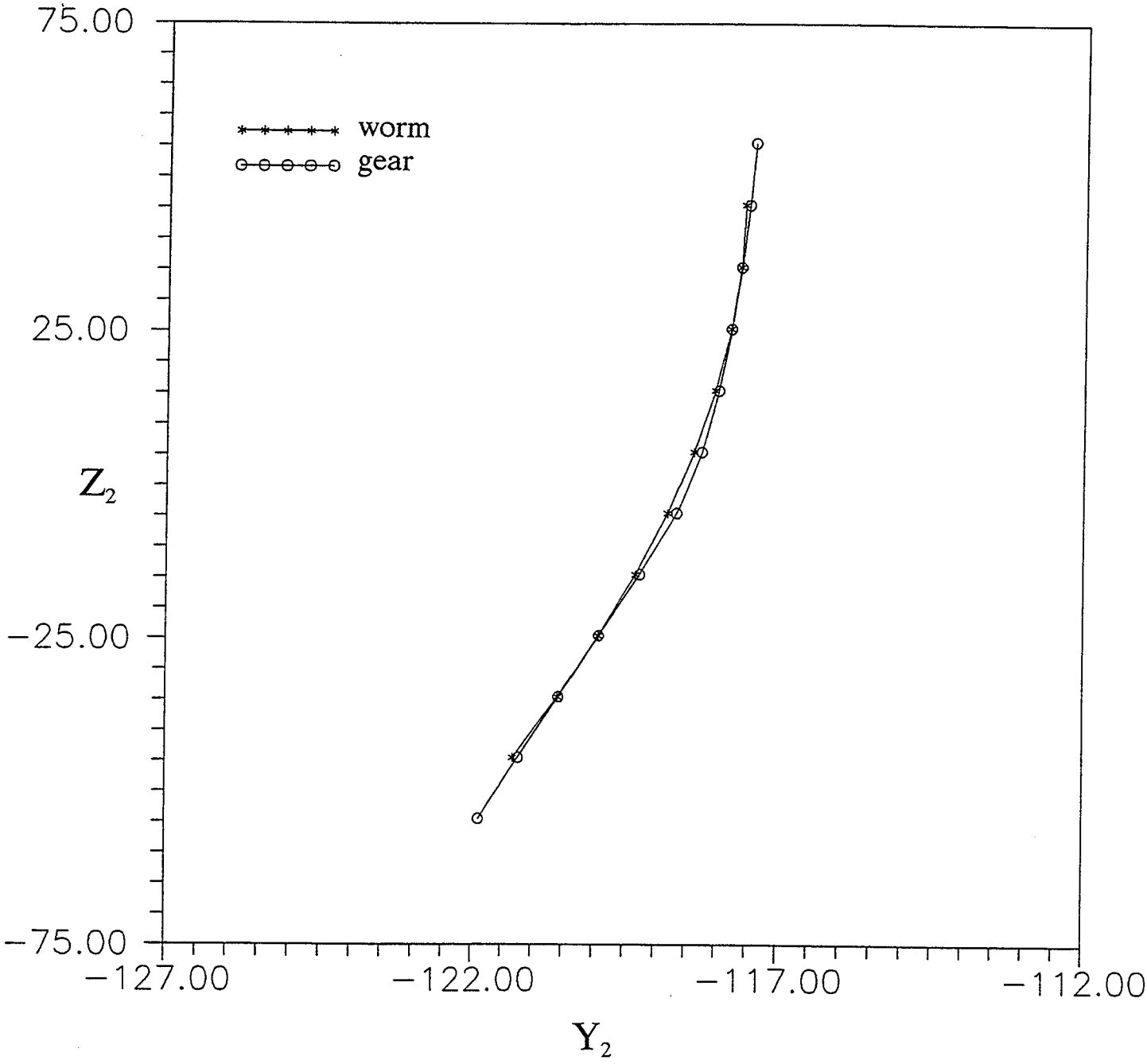

Fig. 30 Clearance function at x_{II} (α_n = 8.5 deg)

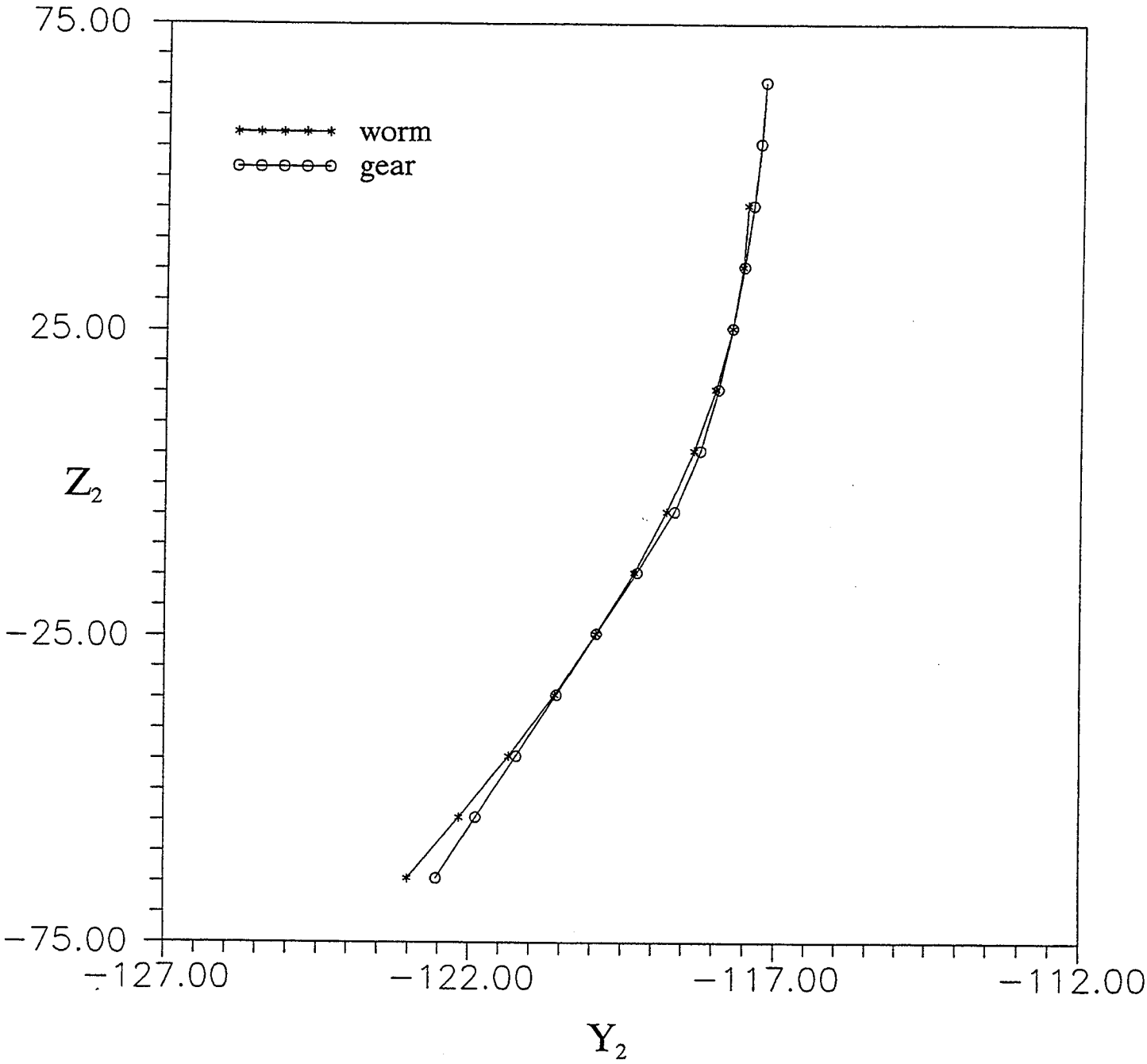

Fig. 31 Clearance function at x_{III} (α_n = 8.5 deg)

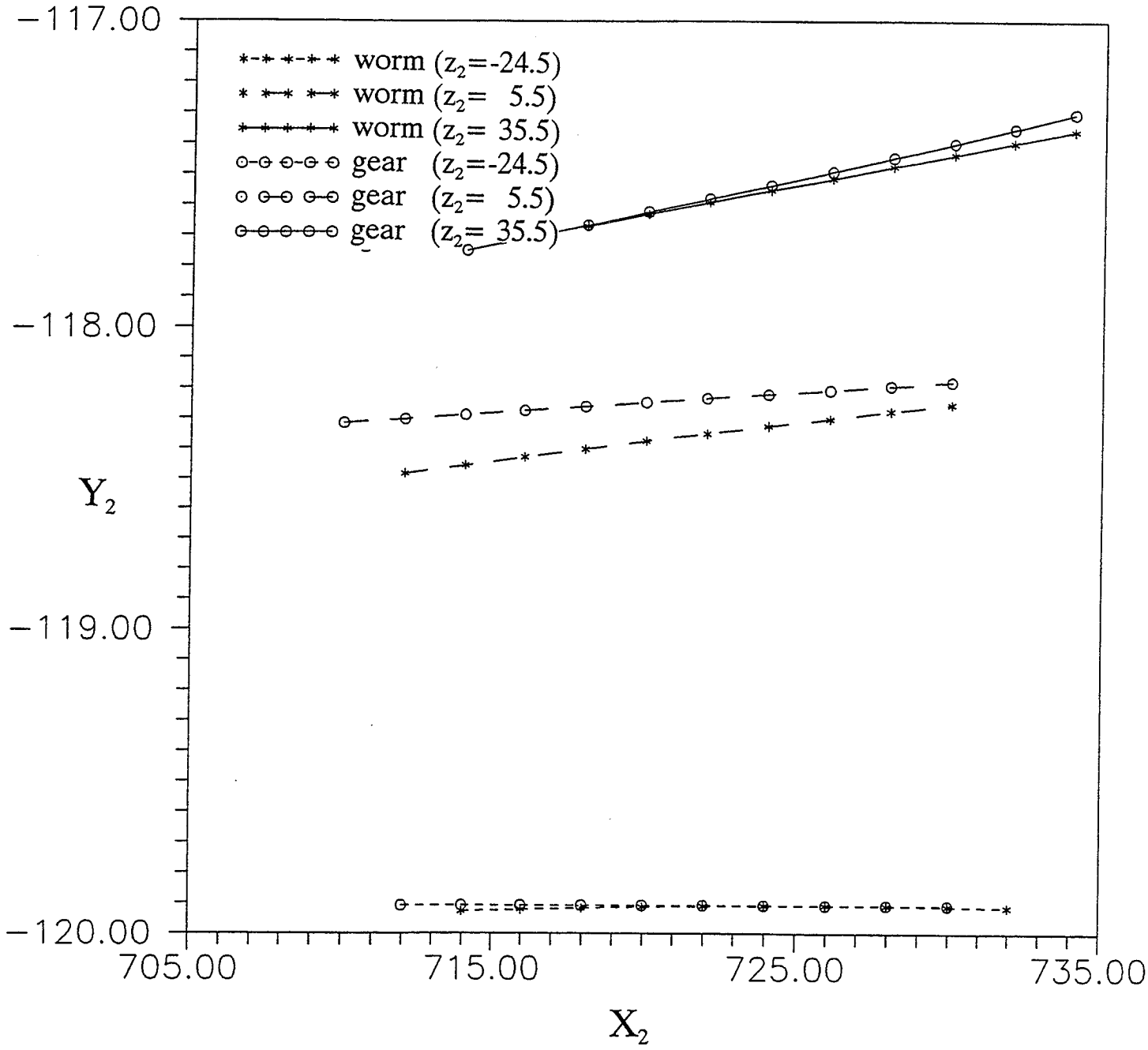

Fig. 32 Clearance function at z_I, z_{II} and z_{III} (α_n = 8.5 deg)

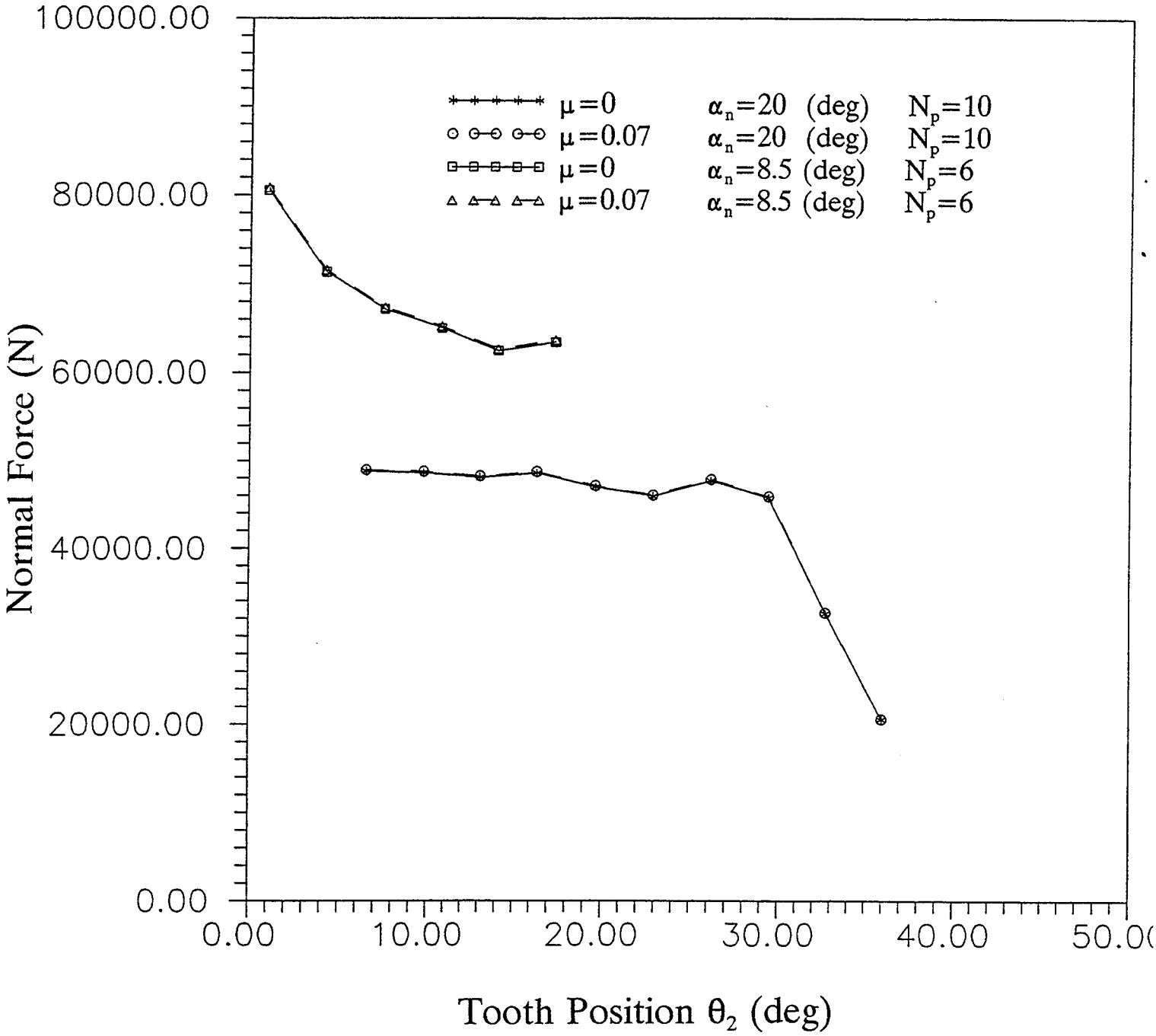

Fig. 33 Comparison of normal force acting on a gear tooth

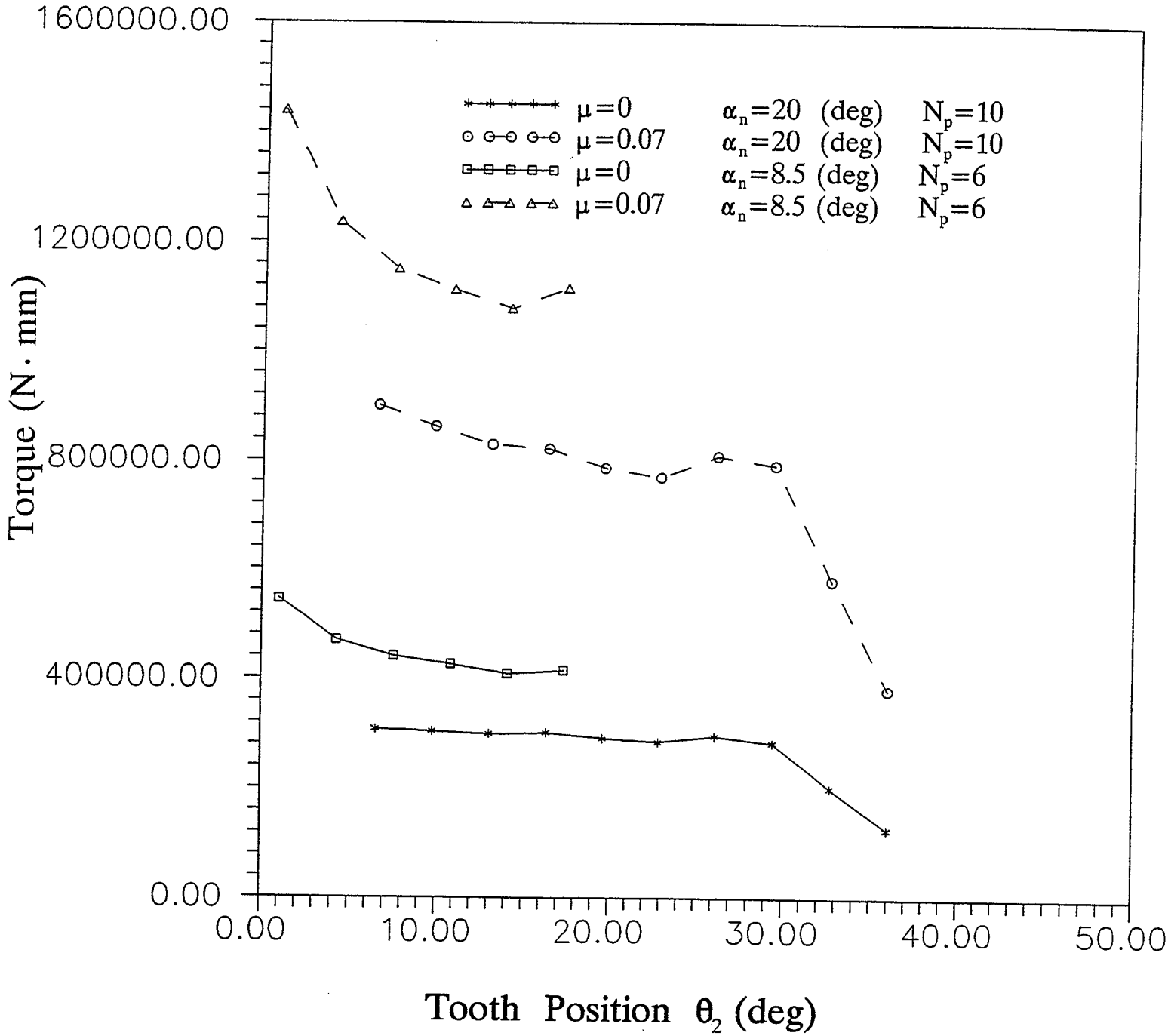

Fig. 34 Comparison of worm torque distribution along the worm tooth

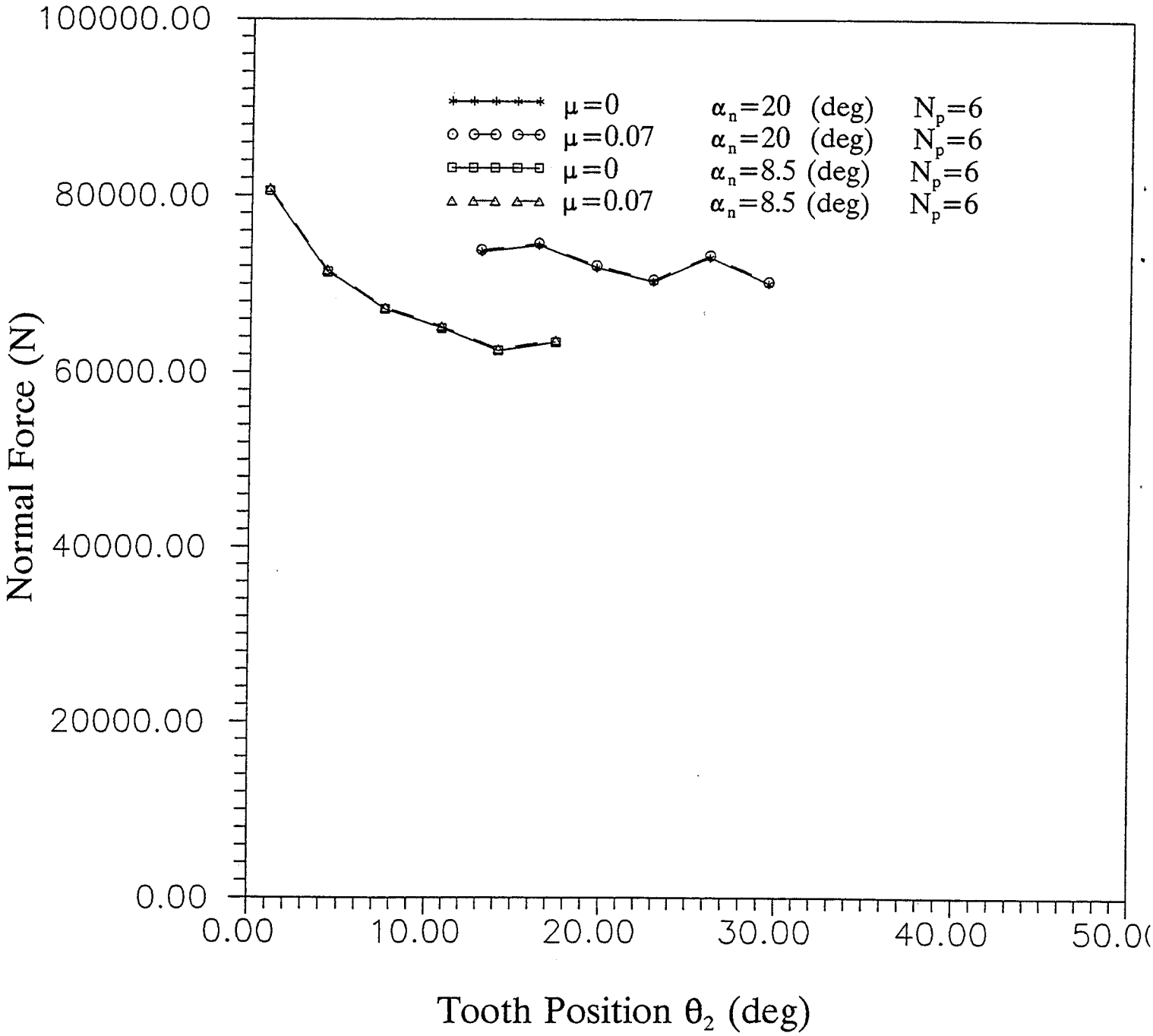

Fig. 35 Comparison of normal force acting on a gear tooth

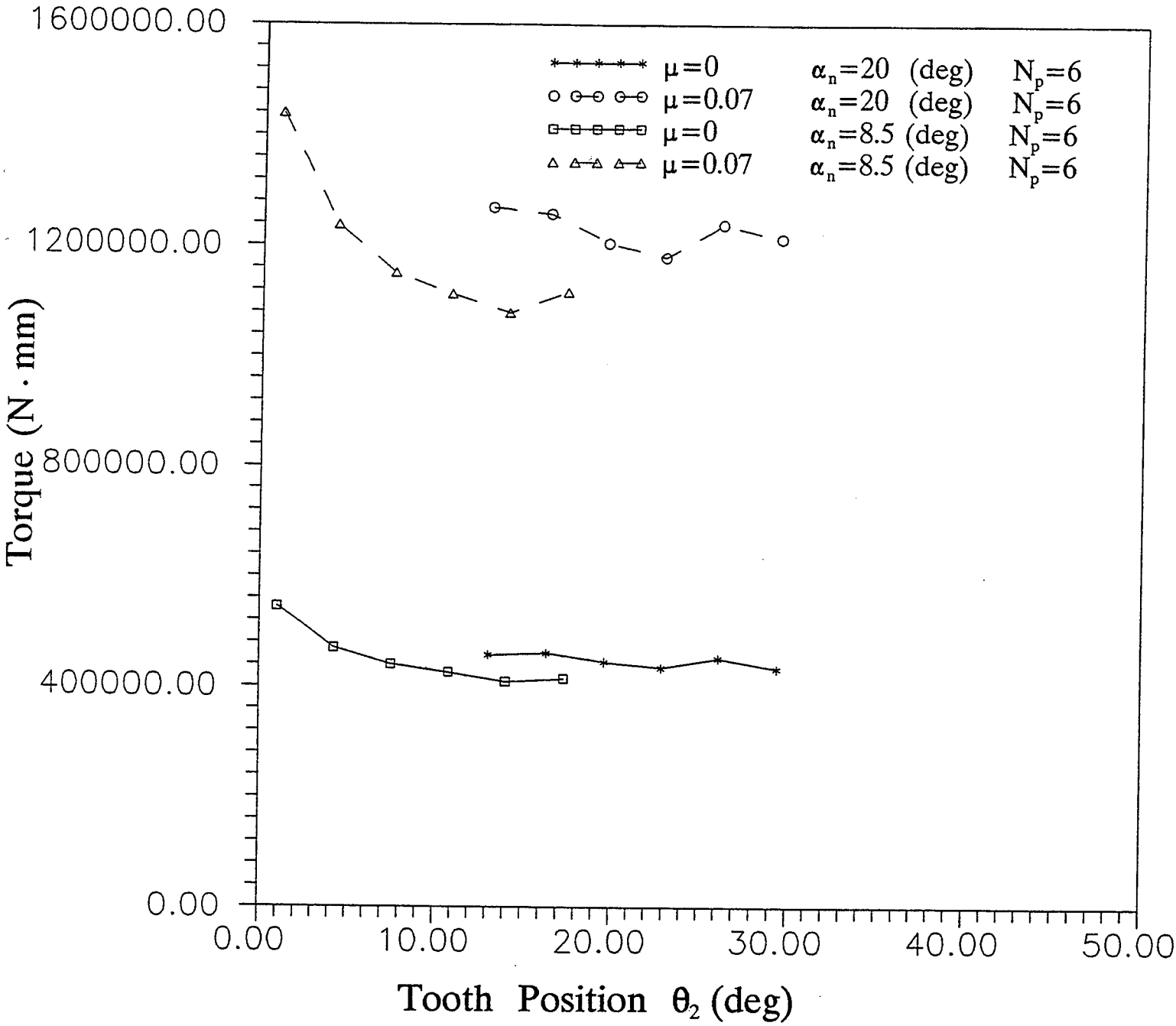

Fig. 36 Comparison of worm torque distribution along the worm tooth

REPORT DOCUMENTATION PAGE

Form Approved
OMB No. 0704-0188

Public reporting burden for this collection of information is estimated to average 1 hour per response, including the time for reviewing instructions, searching existing data sources, gathering and maintaining the data needed, and completing and reviewing the collection of information. Send comments regarding this burden estimate or any other aspect of this collection of information, including suggestions for reducing this burden, to Washington Headquarters Services, Directorate for Information Operations and Reports, 1215 Jefferson Davis Highway, Suite 1204, Arlington, VA 22202-4302, and to the Office of Management and Budget, Paperwork Reduction Project (0704-0188), Washington, DC 20503.

1. AGENCY USE ONLY (*Leave blank*)	2. REPORT DATE	3. REPORT TYPE AND DATES COVERED
	January 1995	Final Contractor Report

4. TITLE AND SUBTITLE

Study of the Kinematic and Load Sharing Properties of Wormgearing With Non-Symmetric Tooth Profiles

5. FUNDING NUMBERS

NAG3–1316
WU–505–62–0J
1L161102AH45

6. AUTHOR(S)

D. C. Sun and Qin Yuan

7. PERFORMING ORGANIZATION NAME(S) AND ADDRESS(ES)

State University of New York at Binghamton
Department of Mechanical and Industrial Engineering
Binghamton, New York 13902-6000

8. PERFORMING ORGANIZATION REPORT NUMBER

E–9303

9. SPONSORING/MONITORING AGENCY NAME(S) AND ADDRESS(ES)

National Aeronautics and Space Administration
Washington D.C. 20546–0001
and
U.S. Army Research Laboratory
Adelphi, Maryland 20783–1145

10. SPONSORING/MONITORING AGENCY REPORT NUMBER

NASA CR–195414
ARL–CR–220

11. SUPPLEMENTARY NOTES

Project manager, David E. Brewe, Vehicle Propulsion Directorate, U.S. Army Research Laboratory, NASA Lewis Research Center, organization code 5140, (216) 433–6067.

12a. DISTRIBUTION/AVAILABILITY STATEMENT

Unclassified - Unlimited
Subject Category 37

This publication is available from the NASA Center for Aerospace Information, (301) 621–0390.

12b. DISTRIBUTION CODE

13. ABSTRACT (*Maximum 200 words*)

The geometry of non-symmetric tooth profiles, i. e. tooth profiles with different pressure angles on the two sides of the tooth, is studied. A feasible non-symmetric tooth profile for application in helicopter transmissions is laid out as the best compromise among several conflicting factors. The non-symmetric tooth profile is then compared with the symmetric tooth profile studied previously. Based on the detailed comparisons it is concluded that the use of the non-symmetric tooth profile would severely limit the face width of the worm, consequently reduce the number of meshing teeth and cause much higher normal load on the individual gear teeth.

14. SUBJECT TERMS

Wormgear; Gears; Transmission; Kinematic; Dynamic; Helicopter; Gearing; Hydrostatic; Loads

15. NUMBER OF PAGES

59

16. PRICE CODE

A04

17. SECURITY CLASSIFICATION OF REPORT	18. SECURITY CLASSIFICATION OF THIS PAGE	19. SECURITY CLASSIFICATION OF ABSTRACT	20. LIMITATION OF ABSTRACT
Unclassified	Unclassified		